UNIVERSIDADE FEDERAL DO CEARÁ

CENTRO DE TECNOLOGIA

DEPARTAMENTO DE ENGENHARIA ELÉTRICA

PROGRAMA DE PÓS-GRADUAÇÃO EM ENGENHARIA ELÉTRICA

MESTRADO ACADÊMICO EM ENGENHARIA ELÉTRICA

MISAEL FELIX QUISPE MAIDANA

COMPARATIVE STUDY BETWEEN PI-AW AND MPC CONTROLLERS WITH GAUSSIAN NOISE IN FEEDBACK LOOP

FORTALEZA

2018

MISAEL FELIX QUISPE MAIDANA

COMPARATIVE STUDY BETWEEN PI-AW AND MPC CONTROLLERS WITH GAUSSIAN NOISE IN FEEDBACK LOOP

Dissertação apresentada ao Curso de Mestrado Acadêmico em Engenharia Elétrica do Programa de Pós-Graduação em engenharia Elétrica do Centro de Tecnologia da Universidade Federal do Ceará, como requisito parcial à obtenção do título de mestre em Engenharia Eléctrica. Área de Concentração: Engenharia Elétrica

Orientador: Prof. Dr. Wilkley Bezerra Correia

Coorientador: Prof. Dr. Bismark Claure Torrico

FORTALEZA

2018

Dados Internacionais de Catalogação na Publicação
Universidade Federal do Ceará
Biblioteca Universitária
Gerada automaticamente pelo módulo Catalog, mediante os dados fornecidos pelo(a) autor(a)

M189c Maidana, Misael Felix Quispe.
Comparative study between PI-AW and MPC controllers with Gaussian noise in feedback loop / Misael Felix Quispe Maidana. – 2018.
75 f. : il. color.

Dissertação (mestrado) – Universidade Federal do Ceará, Centro de Tecnologia, Programa de Pós-Graduação em Engenharia Elétrica, Fortaleza, 2018.
Orientação: Prof. Dr. Wilkley Bezerra Correia.
Coorientação: Prof. Dr. Bismark Claure Torrico.

1. Ruído. 2. Saturação. I. Título.

CDD 621.3

MISAEL FELIX QUISPE MAIDANA

COMPARATIVE STUDY BETWEEN PI-AW AND MPC CONTROLLERS WITH GAUSSIAN NOISE IN FEEDBACK LOOP

Dissertação apresentada ao Curso de Mestrado Acadêmico em Engenharia Elétrica do Programa de Pós-Graduação em engenharia Elétrica do Centro de Tecnologia da Universidade Federal do Ceará, como requisito parcial à obtenção do título de mestre em Engenharia Eléctrica. Área de Concentração: Engenharia Elétrica

Aprovada em: 28 de Março de 2018

BANCA EXAMINADORA

Prof. Dr. Wilkley Bezerra Correia (Orientador)
Universidade Federal do Ceará (UFC)

Prof. Dr. Bismark Claure Torrico (Coorientador)
Universidade Federal do Ceará (UFC)

Prof. Dr. Fabrício Gonzalez Nogueira
Universidade Federal do Ceará (UFC)

Prof. Dr. George André Pereira Thé
Universidade Federal do Ceará (UFC)

This project is dedicated to my family Quispe Maidana and especially to the love of my life, Eva Mamani Tinini.

ACKNOWLEDGEMENTS

I would like to express my deep gratitude to Professor Wikley and Professor Bismark, my research supervisors, for their patient guidance, enthusiastic encouragement and useful critiques of this research work. I want also like to thank Professor Laurinda and Fabricio, for their advice and assistance in keeping my progress on schedule.

I would also like to extend my thanks to all the Group of Brazilian universities *COIMBRA* and the Capes Foundation, for trusting on me for the realization of this specialization at the Federal University of Ceará.

Finally, I wish to thank my parents for their support and encouragement throughout my study.

“A man never knows what he is capable until he tries.”

(Charles Dickens)

RESUMO

O presente trabalho propõe um estudo comparativo entre o controlador PI clássico com estrutura Anti-Windup (PI-AW) e Controle Preditivo basado em Modelo (MPC), ou seja, o controlador GPC-T. Estas duas técnicas de controle são aplicadas em diferentes plantas, considerando as seguintes situações: Presença de saturação no sinal de controle, o qual está relacionado às limitações físicas dos atuadores e à presença de ruído Gaussiano no laço de realimentação. Finalmente, como é bem conhecido no controle do processos, os atuadores geralmente operam perto de seus limites de saturação, por exemplo, o controle de velocidade de um motor elétrico está sempre sob a influência da carga, pois o sinal de controle conduz os atuadores próximos aos seus limites de operação. Portanto, tem-se perda de referência levando a um erro de estado estacionário, o que é indesejável nos processos de controle. Este é o fenômeno *Erro de Rastreamento Induzido por Ruído* **NITE**.

Embora o controlador preditivo GPC tem mostrado um desempenho menor em comparação com o PI-AW, incorporação o polinômio-T, o seja o conhecido controlador GPC-T melhorou consideravelmente a rejeição de perturbações e a atenuação do ruído, quando a saturação é incluída no processo de otimização com restrição, então se diminui o fenômeno NITE.

Para verificar experimentalmente a análise mencionada encima, tem sido escolhido o laço de controle de velocidade de um Motor de Relutância Variável (MRV). Essa planta mostrou ser adequada para a análise, pois possui oscilações mecânicas intrínsecas e o ruído de medição. Portanto, ao escolher corretamente uma velocidade de referência, pode-se levar a máquina a operar muito perto dos limites dos atuadores, enfatizando o efeito de distúrbios e ruídos na operação geral. Então o fenômeno NITE é verificado e sua diminuição pelo controlador GPC-T com otimização analítica para diminuir o esforço computacional no DSP.

Palavras-chave: Ruído. Saturação. PI-AW. GPC-T.

ABSTRACT

The present work proposes a comparative study between the classical PI controller with Anti-windup structure (PI-AW) and a Model Predictive Control (MPC), then the control to be applied is GPC-T. These two control techniques are applied to different plants considering the following situations: Presence of saturation on the control signal, which is related to the real limitations of actuators and the Gaussian noise presence in the feedback loop. Finally, as it is well known in the process control, actuators commonly operate close to their saturation limits, e.g., speed control of an electric motor is always under the influence of the load as consequence the control signal leads the actuators close to their limits. Therefore, loss of reference may happen leading to a steady-state error, which is undesirable in the control processes. This phenomenon is called *Noise Induced Tracking Error* **NITE**.

Although predictive controller GPC has shown poorer performance compared to the PI-AW one, incorporation of the T-polynomial, i.e., the well-known GPC-T controller considerably improved both disturbance rejection and noise attenuation, when saturation is included in the optimization process with constraint, i.e, decreases the NITE phenomenon.

In order to verify the aforementioned analysis experimentally, it has been chosen the speed control loop of a variable reluctance motor (SRM). Such plant has been shown to be suitable for the analysis as it has intrinsic mechanical oscillations and measurement noise. Therefore, by properly choosing a reference speed, one may take the machine to operate very close to the actuators limits, emphasizing the disturbances effect and noises in the overall operation. Then the NITE phenomenon is verified and its decrease by the GPC-T controller with analytic optimization, to decrease the computational effort in the DSP.

Keywords: Noise. Saturation. PI-AW. GPC-T.

LIST OF FIGURES

LIST OF TABLES

LIST OF ABBREVIATIONS AND ACRONYMS

CARIMA	Auto Regressive Integrated Moving Average
DSP	Digital Signal Processor
GPC	Generalized Predictive Control
IAE	Integral Absolute Error
MPC	Model Predictive Control
NITE	Noise Induced Tracking Error
PI	Proportional Integral
PID	Proportional Integral Derivative
PWM	Pulse Width Modulation
SISO	Single Input Single Output
SRM	Switched Reluctance Motor Drives
TV	Total Variation

LIST OF SYMBOLS

Δ	discrete-time integrator
$\Delta u(t)$	control weighting
ε	hysteresis width
λ	control weighting
ω_m	angular velocity
θ	rotor position
d	transportation delay
θ_{off}	disconnection angle
θ_{on}	shooting angle
f	free answer of the system
G_{pv}	speed plant model
i_n	phase current
I_{ref}	reference current
K_p	proportional gain
K_i	integral gain
K_a	gain action of mitigate windup
N	Prediction horizon;
N_1	minimum prediction horizon
N_2	maximum prediction horizon
N_u	control horizon
$n(t)$	noise signal
$P(s)$	plant model
T_s	sampling time
t	time
$u(t)$	control signal
V_{dc}	voltage

$w(t+j)$	reference future
y	output signal
z_c	position of zero controller
ZL	Impedance

CONTENTS

1 INTRODUCTION

Currently, in the industrial environment, it is very common the need of controllers with easy operation and simple adjustment. Therefore, the control engineering has involved the development of methods and techniques that are constantly evolving in order to improve performance, efficiency and effectiveness in the control loop (NUNES, 2001).

Since its introduction the Proportional-Integral-Derivative PID controller has been by far the most extensively controller for industrial applications (ASTRöM; HäGGLUND, 1995). Its success is mainly due to its simple structure and ease parameters tuning for a wide range of different real processes.

Many processes may present failures in system performance which usually cannot be predicted. These failures are derived of certain restrictions to which most industrial processes are subjected or under certain specific working circumstances, but these are not considered during the design of the controllers.

In real processes there are usually physical limitations by part of the actuators, these are responsible for translating the control signal granted by the control law to run it on the plant. Few examples include industrial communication between control equipment and final actuators, which commonly use the HART (Highway Addressable Remote Transducer) protocol, that only operates in the current range of 4 to 20 *mA* (GUERRERO *et al.*, 2009). A solenoid valve cannot open more than 100% and a motor cannot work beyond the rated speed. These limitations may be named saturation (VISIOLI, 2006).

The actuator saturation is the most common and significant of the non-linearity found in control system. In the literature, there are several examples where by neglecting them the saturation has led to crucial difficulties and put in danger the overall stability of the system. For example, it has also been blamed as one of several unfortunate mishaps leading to the 1986 Chernobyl nuclear power plant disaster where unit 4 melted down with dreadful consequences (STEIN, 1989; KOTHARE, 1997).

If the controller has integral action and saturation associated with the control signal it may appear the windup phenomenon when the actuator becomes saturated occurs that the feedback loop is interrupted, the system operates as an open loop, i.e., the integrative action continues to integrate this error increasing it considerably giving an overshoot note that it may be very harmful since it may affect closed-loop stability. This effect is mitigated by considering Anti-Windup control strategy. For a classic PID controller it changes for the PID-AW controller

(OGATA, 1997).

The noise is present in the physical processes, which tends to be of a higher frequency with relation to process dynamics. Sources of signal noise are due to: Electrical interference, Jitter (clock related irregularities such as variations in sample spacing), quantifying of signal samples into overly-broad discrete “buckets” from low resolution or improperly specified instrumentation (e.g. too-large measurement span relative to operating range), vibrations of the actuators (bad adjustment of equipment) or the same plant to be controlled presents vibrations (KIM *et al.*, 2015), (MOHAMMED, 2017).

1.1 Motivation

In the study of the classical control technique PI-AW, recently it was mentioned for a stable plant in open loop by (EUN; S., 2015), when there is the presence of Gaussian noise in the feedback loop and saturation of the control signal. These characteristics induce the loss of reference tracking, consequently, there is a steady-state error. This phenomenon is called *Noise Induced Tracking Error* **NITE** by (EUN; S., 2015). Later also it was analyzed for different types anti-windup structures with PI controller, where show that **NITE** phenomenon occurs by (LEE; EUN, 2016).

For the mentioned, it is observed that the tuning parameters of the PI-AW controller are not appropriate, therefore to correct the phenomenon is necessary to readjust of the controller parameters to eliminate this phenomenon NITE. However, this process changes the projected response of system and it is not industrially desired because time-consuming requires as well as the discontinuity of process in question.

The hypothesis is if this phenomenon NITE can occur in other controllers. Then the Model Predictive Control MPC will be studied, because is an advanced method of process control that is used to control a multi-input, multi-output process while satisfying a set of constraints. It has been in use in the process industries in energy generation, ship building, chemical plants and oil refineries since the 1980 (ALLGöWER; ZHENG, 2000). In recent years it has also been used in power system balancing models and in power electronics (SHORT; ABUGCHEMN, 2017).

So will be studied the MPC controller under the same operating conditions of the PI-AW controller as saturation for the control signal and Gaussian noise in the feedback loop and if this NITE phenomenon occurs.

1.2 Objetives

In view of the exposed in the previous section, it develops the overall objective and Specific objectives to achieve in the present thesis.

1.2.1 Overall objective

The objective is to perform a comparative study of performance of the PI-AW and MPC controllers to different plants: stable, integrative, SRM, under the presence of noise in feedback loop. For the design of the controller MPC it applies the GPC controller which will incorporate the application of the T-polynomial to reject step-like disturbances and noise attenuation, i.e., a GPC-T controller.

1.2.2 Specific objectives

- Review of control strategy PI-AW and GPC-T.
- To perform simulations of the designed controllers applied the presence of noise in the feedback loop.
- To implement control techniques studied in the control of speed of the SRM.
- Compare performance of controllers, through the performance indices IAE, TV.

1.3 Scientific Production

Throughout the development of this thesis was published the article:

Maidana,M.Q. & Correia,B.W. & Torrico, B.C. & Nogueira,F.G., "Comparative study of PI-AW and MPC-T controllers, with feedback noise applied for speed control to a Switched Reluctance Motor (SRM)", accepted in Brazilian Power Electronics Conference (COBEP-2017)

1.4 Thesis Overview

In order to present the developed aspects throughout the research, this thesis it was divided into 5 Chapters including this introduction, then is organized as follows:

- Chapter 2:

This chapter will explain two situations recurrent in the control systems as the Windup effect

and the noise measurement.

- Chapter 3

This chapter is divided into three subsections:

First place, to review of the classic controller PI with Anti-Windup structure, i.e., a PI-AW. Second place, it is a review of the MPC control structure from which it decomposes the Generalized Predictive Controller (GPC). Finally, cite the definitions of the performance indices IAE and TV.

- Chapter 4

This chapter is divided into two sections:

First place, compare the PI-AW and GPC-T controllers for the stable and integral plant in form of simulations. Second place has been validated the comparison of the PI-AW and GPC-T controllers experimentally through the speed control of a Switch Reluctance Motor (SRM). So these analyzes are validated by performance indices.

- Chapter 5:

Are presented the corresponding main conclusions of work performed and future work to follow. Continuing with the references used with the list of articles and research projects related to the research.

2 INFLUENCE FACTORS IN THE CONTROL LOOPS

This chapter discusses two influence factors recurring in the process control loops, such as internal (Windup) and external (noise measurement), whose influence may vary depending upon the process. The Windup effect is studied is many associated with the integral action due the controller and saturation for the control signal. Then the presence of noise measurement in the feedback loop is highlighted. Finally, an example is discussed for a stable plant with PI controller with Anti-windup effect, i.e., a PI-AW controller. It also contemplates the presence of Gaussian noise present in the feedback loop, so one can observe this particular phenomenon.

2.1 Windup effect

One of the most commonly neglected and often undetected problems in control loop is the wind-up effect. This occurs when a controller with integral action exceeds the physical limits of the actuator. In this work, only the amplitude limitation is considered in the actuator, which is quite common, being described by the following nonlinear function:

$$\hat{u} = \text{sat}(u) = \begin{cases} U_{min} & if \quad u < U_{min} \\ u & if \quad U_{min} \leq u \leq U_{max} \\ U_{max} & if \quad u > U_{max} \end{cases}, \tag{2.1}$$

where U_{min} and U_{max} are the minimum and maximum signals allowed by the actuator. It can be represented as in Figure 1.

Figure 1 – Limitation in the amplitude of control signal.

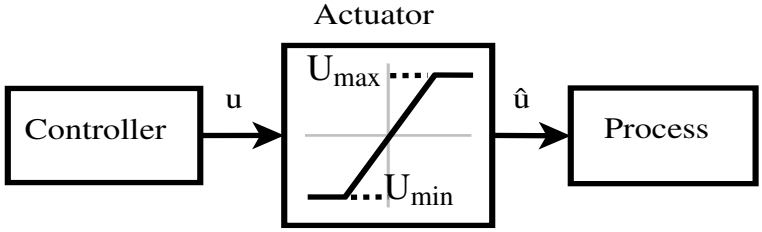

Source: Author.

A classic example of Windup control known as integrator Windup is illustrated in the following Figure 2.

Figure 2 – Control loop block diagram.

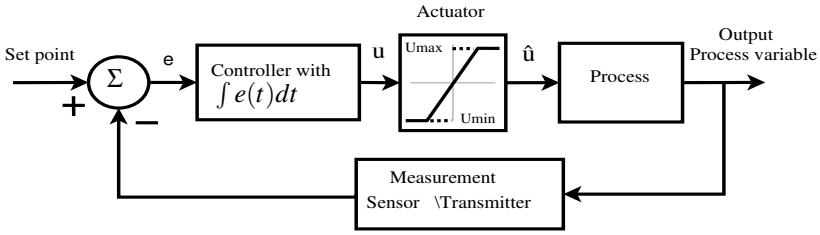

Source: Author

If the set point receives a sudden positive step command, the error, e, will initially be positive as the system begins to respond to the actuator. If the rate of integration is fast with respect to the speed of the system, the integrator output may exceed the saturation limit of the actuator but continue to grow in size itself (see Figure 3 Integral control action). When the system output finally reaches the commanded value, the sign of the error reverses causing the integrator to begin "winding" down. But the output of the integrator, far beyond the operating range of the actuator, takes such a significant amount of time to recover within the operating range of the actuator and so causes a lag in response. This process can repeat itself as a limit cycle, or eventually converge towards the commanded value depending on the set gain and system response (DORF; BISHOP, 2011).

Figure 3 – Windup effect response.

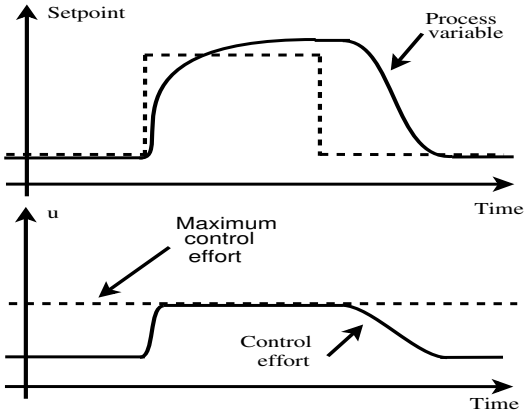

Source: (DORF; BISHOP, 2011)

The Windup effect can occur in electronic, mechanical or software components in a control loop. It may also occur in any control element that contains memory. A first-order lag or any filter can create Windup. If the designer permits Windup to occur, the closed loop system can exhibit excessive overshoot, sustained oscillations, and/or lengthy settling times (HU; LIN, 2001a). Finally, overshoot may be due to a dominating possession of zero that has the process.

In order to understand the Windup phenomenon the following example is presented

for a PI controller (see Figure 4).

Figure 4 – PI controller with saturation.

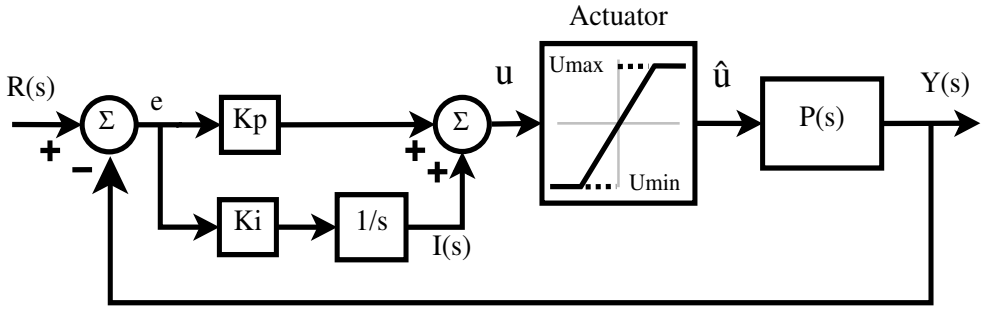

Source: Author

Where the chosen plant is $P(s) = \frac{1}{(3s+1)}$ and the controller is tuned as $K_p = 5$, $K_i = 3$. The control signal delivered to the saturator is given by:

$$\mathrm{u(t)} = K_p \mathrm{e(t)} + K_i \int_0^t \mathrm{e(t)} dt, \tag{2.2}$$

then when signal u passes through the saturator (see Equation (2.1)), signal û is delivered to the process, whose graphs are given in the Figures 5, 6, 7.

Figure 5 – System response Y(s).

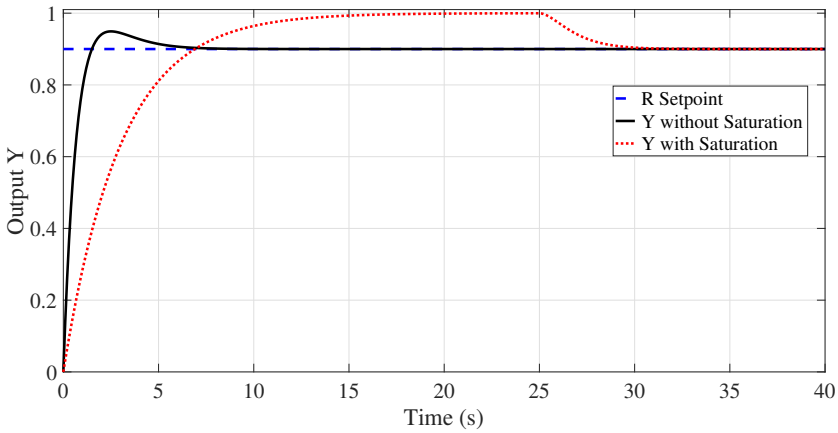

Source: Author

Figure 6 – Control signal û.

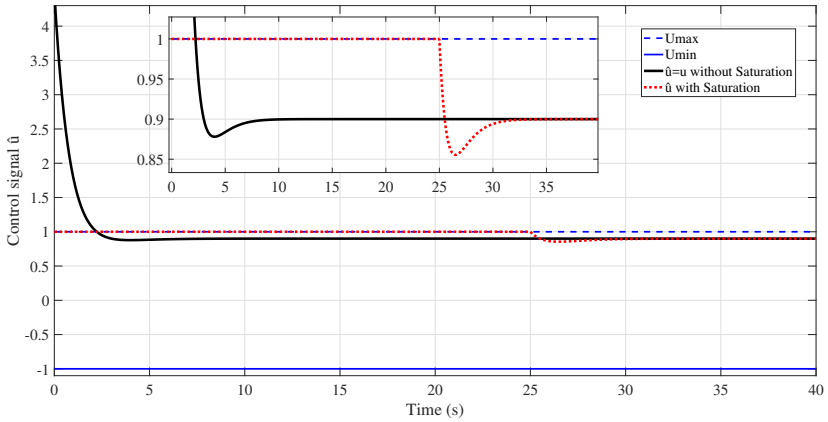

Source: Author

Figure 7 – Behavior of integral term I.

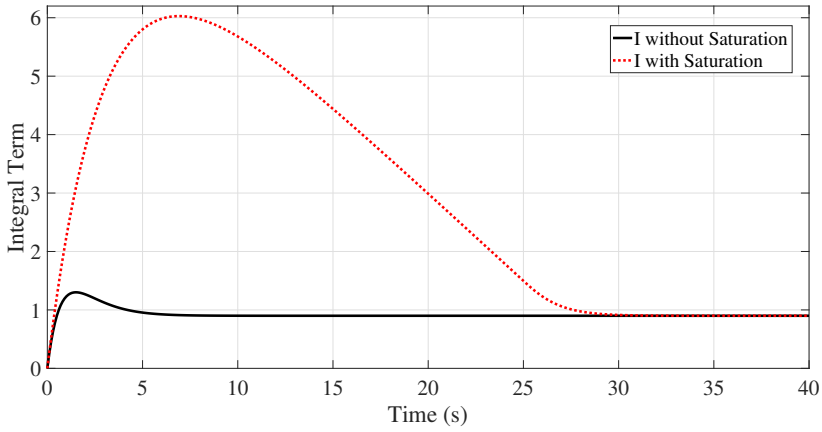

Source: Author

As shown in the Figure 7 there is an overshot (red color), which is due to the integral action of the PI controller, this is the Windup effect.

Very often a design will look good in simulation or on paper, but when implemented fails to perform as expected. Unknowingly, the designer will attempt to fix the problem by reducing gains of the controller. This slows integration rates to match the system speed and can prevent Windup in the closed loop, but at the expensive of reduced speed of the closed loop response (OGAWA *et al.*, 2010).

In order to prevent Windup effect, the operating range of control elements should be limited to the range of the devices they are driving. This helps provide instant recovery when the control error changes sign. For complex control algorithms limiting specific control components in software becomes a simpler task than with electronic controls.

A classic solution to the phenomenon windup is known as Anti-Windup is known as back-calculation, tracking, or classical Anti-Windup. The method was first described by (FERTIK; ROSS, 1967). This Anti-Windup algorithm is detailed in chapter 3 of this thesis.

2.2 Noise in the Process

Noise may be seen as any unwanted high-frequency signal that is added in the feedback loop. There are multiple sources of noise, some external as a motor of a car, elevator, mobile phone, etc. and others internal as thermal noise, parts wear, etc. (HANSLER; SCHMIDT, 2004).

In an industrial plant by the conditions physical existing the noise is present, therefore must be considered its effects in the controller design. The nature of noise sources is random for which it is suitable to consider a stochastic approach. Within this context, one may highlight (HANSLER; SCHMIDT, 2004):

- White noise where its energy density is distributed equally in all the frequency range. Example: Thermal noise caused by a random motion of the electrons of a metal with the temperature (see Figure 8).
- Impulsive Noise, which is mainly produced at irregular intervals with very pronounced peaks of short duration. Usually has external origin as: lighting of a light, relays, etc. (see Figure 8).

Figure 8 – Different types of noise.

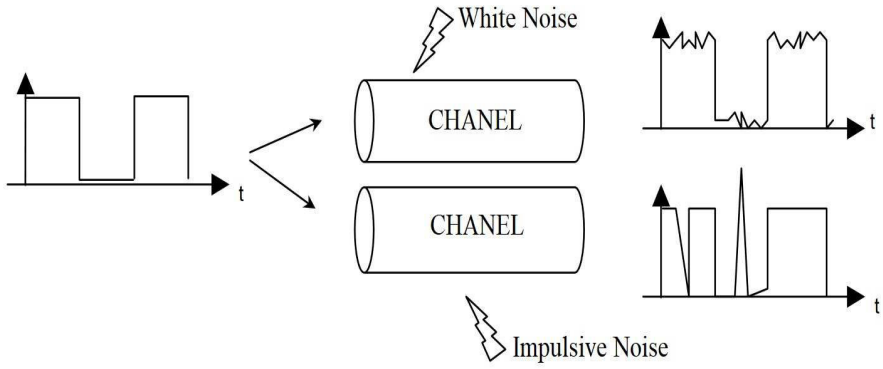

Source: <http://trajano.us.es/~rafa/ARSS/apuntes>

The electrical noise give for equipment (motors, Transistors, etc) or sensors generally have a similar behavior to white noise, this can be considered also as a Gaussian noise due to the probability of repetition (HANSLER; SCHMIDT, 2004).

So the white noise is a Gaussian noise (see Figure 9), then it begins with determining the likely values of statistics measures that character the level of noises in the system (LI, 2005). It is well known that the probability of a Gaussian random variable X fall in the interval $[m_x - a, m_x + a]$ is:

$$P[m_x - a \leq X \leq m_x + a] = erf\left[\frac{a}{\sqrt{2}\sigma_x}\right], \tag{2.3}$$

where m_x is the mean, and σ_x^2 is the variance and $erf(.)$ is the error function (also called the Gauss error function) is a special function (non-elementary) of sigmoid shape that occurs in probability, statistics, and partial differential equations describing diffusion. It is defined as:

$$erf(x) = \frac{2}{\sqrt{\pi}} \int_0^x e^{-t^2} dt, \tag{2.4}$$

in statistics for non negative values of x, the error function has the following interpretation: for a random variable Y that is normally distributed with mean 0 and variance 1/2, $erf(x)$ describes the probability of Y falling in the range $[-x, x]$ (ANDREWS, 1998).

Let us suppose that signal to noise at the input end of the system is 5 (Signal-Noise Ratio), this means that :

$$SNR = \frac{Signal \quad Amplitude}{Noise \quad level} = 5. \tag{2.5}$$

Figure 9 – Gaussian noise probability function

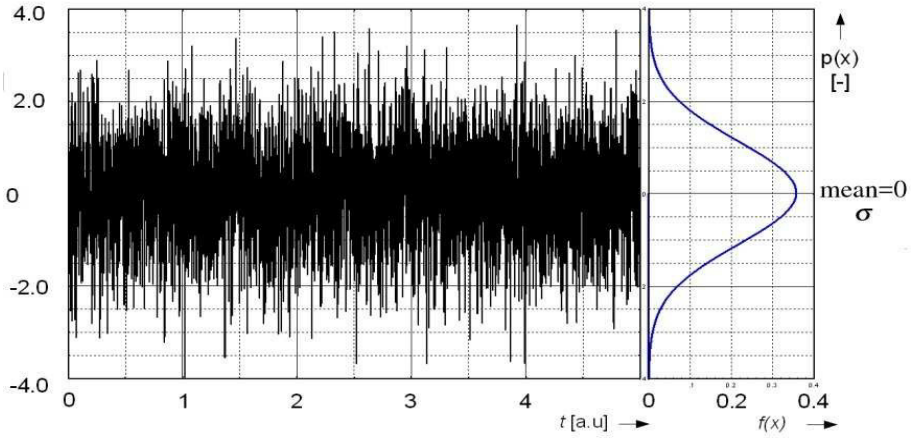

Source: <http://www.equaphon-university.net/senales-de-prueba/>

For example, if signal magnitude is 0.5, the noise level will be 0.1 mm. Next, if the probability of $P[-0.1 \leq X \leq +0.1] = 0.95\%$, invoking command line $>> erfinv(0.95)$ in

Matlab yields: $>> erfinv(0.95) = 1.3859$. Therefore, σ_x can be calculated as follows:

$$\frac{0.1}{\sqrt{2}\sigma_x} = 1.3859 \Longrightarrow \sigma_x = 0.0510. \tag{2.6}$$

With the exposed previously, may be cited follows example with PI-AW controller (should be noted that this control strategy will be studied in detail in Chapter 3), see Figure 10.

Figure 10 – PI-AW controller with noise in feedback loop.

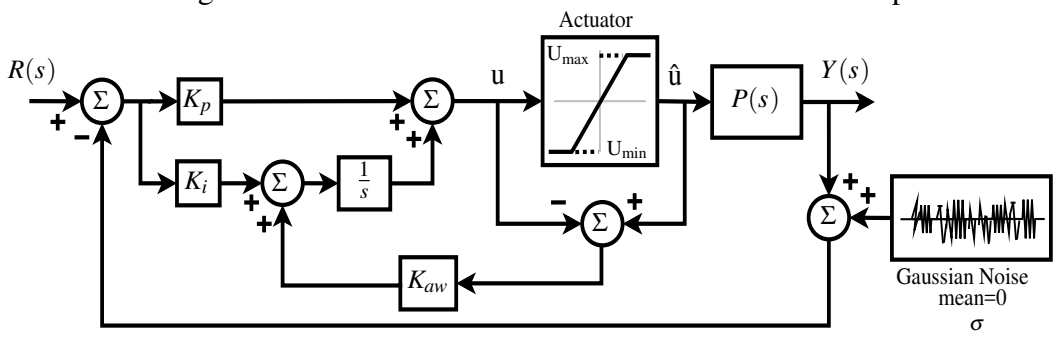

Source: (EUN; S., 2015)

Where the chosen plant is $P(s) = \frac{1}{(3s+1)}$ with $T_s = 0.1[s]$. The controller is tuned as $K_p = 5$, $K_i = 3$, $K_{aw} = 1$. The reference or set-point is $R(s) = 1$ and the limits saturation are: $\mathrm{U_{max}} = 1$ and $\mathrm{U_{min}} = -1$. The Gaussian noise with standard deviation is $\sigma = 0.1$ with $mean = 0$ for the feedback loop.

First, the effectiveness of the PI-AW controller would be checked without the presence of Gaussian noise in the feedback loop, i.e., standard ($\sigma = 0.0$).

Figure 11 – System response without noise

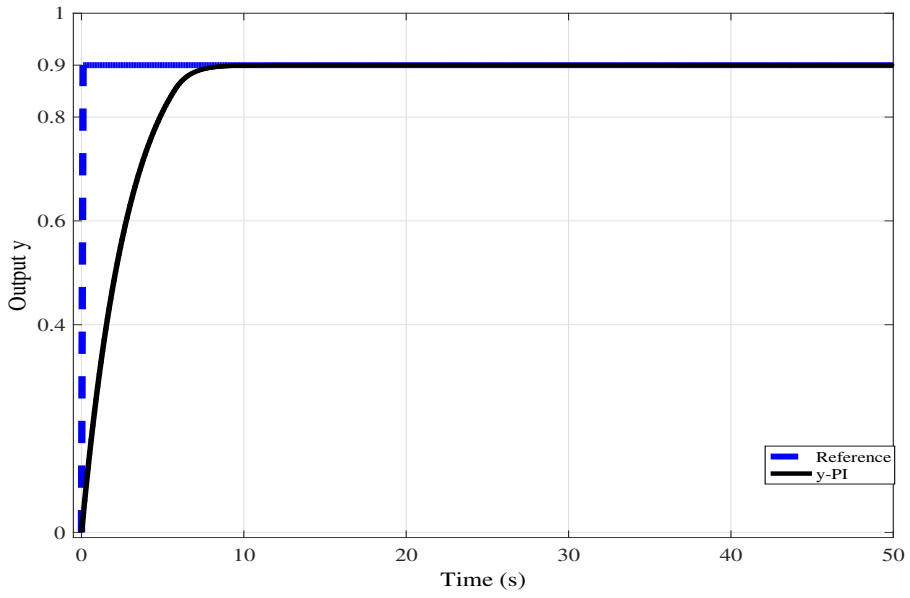

Source: Author

Figure 12 – Control signal given to the plant

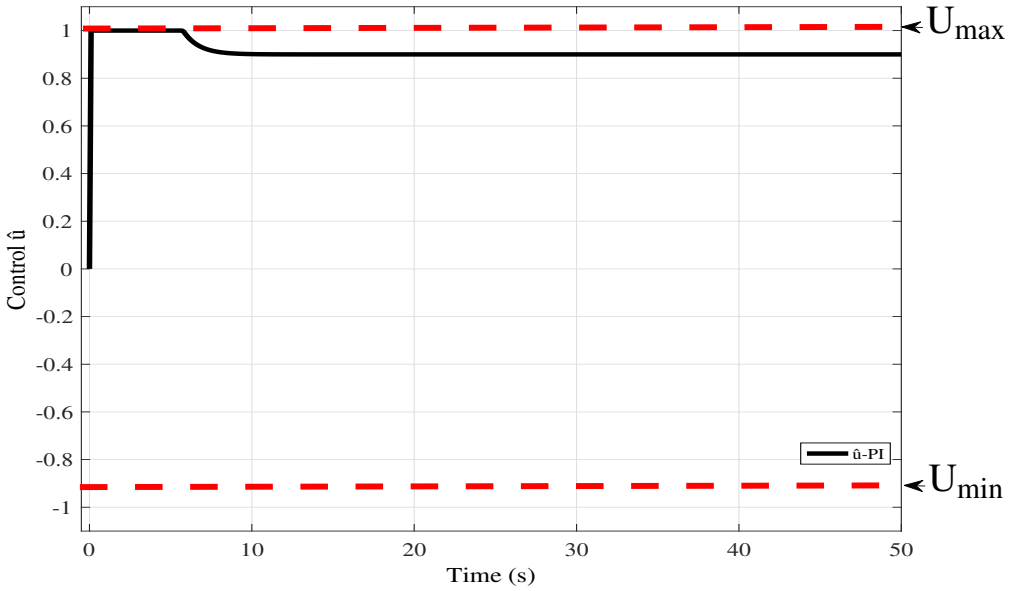

Source: Author

From Figures 11 and 12 show that the controller responds properly obtaining a steady state error equal to zero, but the control signal to stay near the upper limit.

Now under the presence of Gaussian noise the system response (see Figure 10). Where it can observe (see Figure 13.) the loss of reference tracking, which leads to a nonzero steady-state tracking error for this control. Then this is the NITE phenomenon by (EUN; S., 2015), which is due to the saturation of the noise peaks (see control signal Figure 14), that instant of noise peaks the system goes into non-linearity.

Figure 13 – System response with noise.

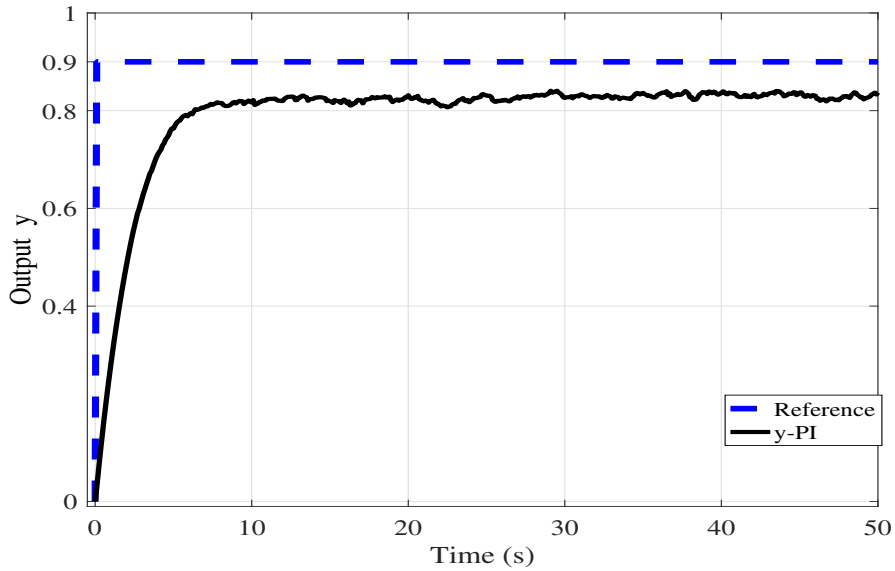

Source: Author

Figure 14 – control signal given to the plant.

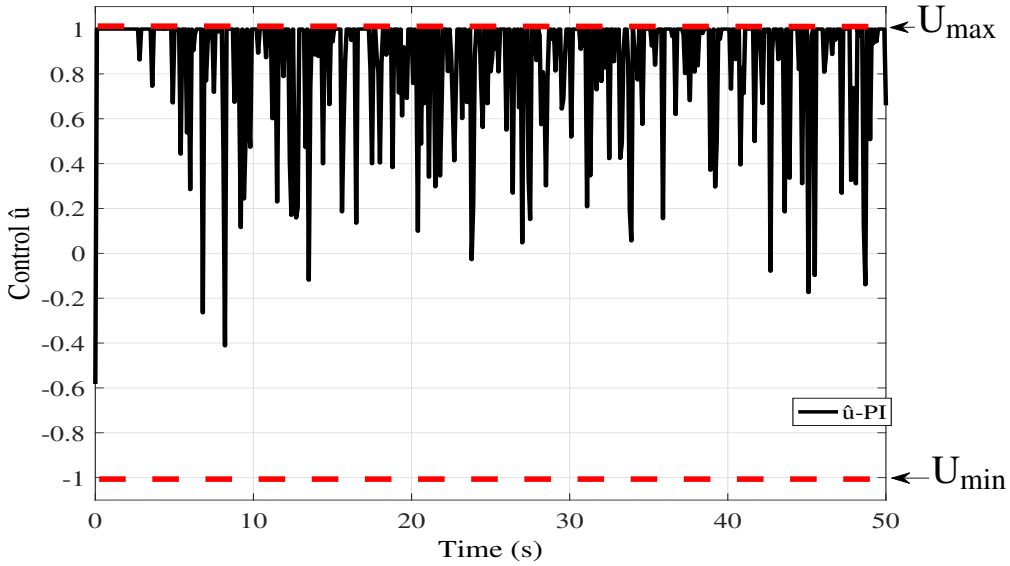

Source: Author

Steady-state error present in the system response (see Figure 13) depends on the Gaussian noise measurement power and this depends of the standard deviation σ. Therefore, for a PI-AW control under the operating conditions aforementioned, it has been shown that measurement noise leads to a nonzero steady-state tracking error, in other words, the presence of the NITE phenomenon (LEE; EUN, 2016). May be observed in the Figure 14, the control signal is limited for the saturation this may decrease the useful life of the actuator.

3 CONTROLLERS DESIGNS

In this chapter will be performed the theoretical foundation of the controllers addressed in the present work: Firstly place, it is explained the strategy of the classical PI controller and its respective Anti-windup structure, i.e., PI-AW and the parameters tuning. Secondly place, for MPC controller, it will be made a brief introduction of its evolution, up until the GPC control. It should be noted that there will be two forms of optimization as numerical and analytically, which is used in the present work. Finally, will review the concepts of performance indices TV, IAE, which will help us to relate a comparison between the controllers described in this chapter.

3.1 Proportional Integral Control

The PID is a controller that have techniques consolidated projects that determine the values of gains proportional, integral and derivative based on the final characteristics desired of the closed loop system as time of settlement and overshoot (OGATA, 1997).

The subsection will be studying the Anti-Windup technique for the PI controller, besides explaining the cause of the Windup phenomenon for this controller.

3.1.1 PI Control Structure

The structure of PI controller is showed in Figure 15:

Figure 15 – Structure of the PI controller.

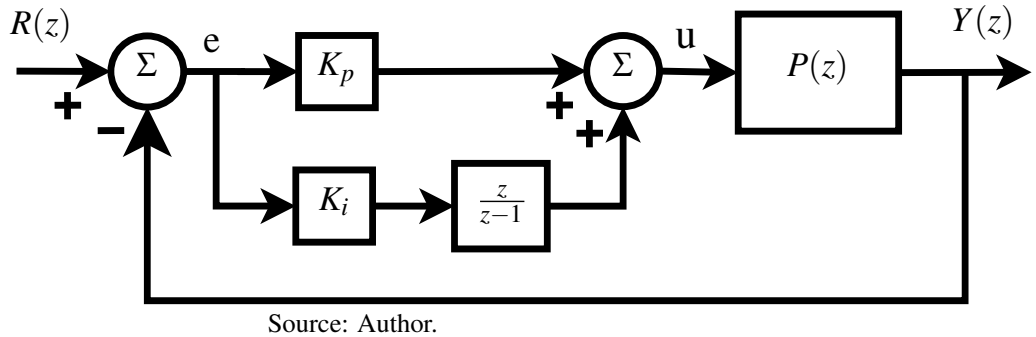

Source: Author.

As it can see from Figure 15, in order to make the output value reach the reference value, the error is minimized by PI controller and with its respective tuning.

The PI control is given by the following Equation (3.1) in the frequency domain.

$$C_{PI}(s) = K_p + \frac{K_i}{s}, \tag{3.1}$$

or in discrete-time equivalent is:

$$C_{PI}(z) = K_p + \frac{K_i z}{(z-1)}. \tag{3.2}$$

Then the equation of output of the PI controller in the time is:

$$\mathrm{u(t)} = K_p \mathrm{e(t)} + K_i \int_0^t \mathrm{e(t)} dt, \tag{3.3}$$

or in discrete-time equivalent is:

$$\mathrm{u}(z) = K_p \mathrm{e}(z) + K_i \frac{z}{z-1} \mathrm{e}(z), \tag{3.4}$$

where $R(z)$ is set-point of the system at time t, $\mathrm{e(z)}$ is error of the system at time t, $\mathrm{Y(z)}$ is result of output of the plant at time t. So controller is based on two parameters which are:

- Proportional Gain Constant K_p:

In proportional control, the actuating signal for the control action in control system is proportional to the error signal. The error signal is being the difference between the reference input signal and the feedback signal obtained from the output. For satisfactory performance of a control system, a convenient adjustment has to be made between the maximum overshoot and steady state error. Through the help of proportional constant without sacrificing the steady state accuracy, the maximum overshoot can be reduced to same of actuating signal.

Figure 16 – Proportional control action.

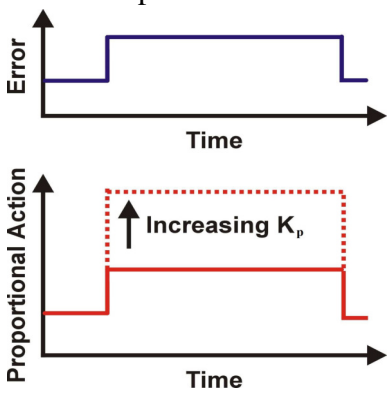

Source: Author.

- Integral Gain Constant K_i:

For integral control action, the actuating signal consists of proportional-error signal added with integral of the error signal. By the help of an integrator is reduces the steady state errors through low frequency compensation. So the integral term will do the actual variable will track the reference more quickly. $K_i = 1/T_i$ represents the integrative time.

Figure 17 – Integral control action.

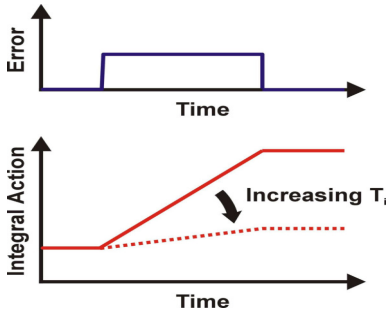

Source: Author.

3.1.2 Controller adjustment methods

In the theory of control, there are different tuning methods for the parameters of the PI or PID control being used (ZIEGLER; NICHOLS, 1942; COHEN; COON, 1983; LOPEZ *et al.*, 1976). Therefore, it will cite the method used in the present work.

3.1.2.1 Root Locus Method

The study Root Locus has demonstrated for years one of the most useful tools in the synthesis of controllers. Then the design of a controller consists of placing the poles and zeros of the transfer function of the system in closed loop, in the most convenient positions in order to achieve a response according to certain specifications, generally in the time domain. then is described is the method through the following steps (RAMAKRISHNAN, 2017):

a) This defines the graph in the z plane of all the poles and zeros of the closed-loop transfer function.

$$1 + C_c(z)P(z) = 0 \tag{3.5}$$

where $C_c(z)$ is the regulator implemented in the digital controller and $P(z)$ is the transfer function of the plant in the z-plane.

b) Module Condition

$$|C_c(z)P(z)| = 1 \tag{3.6}$$

c) Condition of Angle or Phase

$$Ang(C_c(z)P(z)) = (2n+1)\pi rad. \tag{3.7}$$

As shown in section 4.3.2 through the process of speed loop identification, the system can be satisfactorily represented for a model of first order with integrator:

$$G_{pv} = \frac{K_{pv}}{z-1}. \tag{3.8}$$

The PI discrete controller is represented by Equation(3.9).

$$G_c(z) = \frac{K_c\,(z-z_c)}{(z-1)}, \tag{3.9}$$

where K_c and z_c represent controller gain and controller zero position respectively. The open-loop function $L_c(z)$ of the system will be:

$$L_v(z) = \frac{K_c K_{pv}(z-z_c)}{(z-1)^2} = \frac{K_1(z-z_c)}{(z-1)^2}, \tag{3.10}$$

being $K_1 = K_c K_{pv}$.

The transfer function closed-loop have two real poles and identical z_p there is a controller with a fast response and without overemphasis. The equation characteristic of system is expressed in Equation (3.11).

$$z^2 + (K_1 - 2)\,z + (1 - K_1 z_c) = 0. \tag{3.11}$$

Thus, solving Equation (3.11) through the Bhaskara formula and comparing with the equating z_p it observes that the gain of the open loop K_1 is related to the poles position by the following Equation (3.12).

$$K_1 = 2 - 2z_p. \tag{3.12}$$

Through the discriminant of Equation (3.11) and using Equation(3.12) it obtains the expression that determines the zero position of controller:

$$z_c = -\frac{K_1 - 4}{4}. \tag{3.13}$$

Therefore, the determination the poles position of the closed loop can be determined PI controller for the speed loop (SILVA, 2013).

3.1.3 Anti-Windup PI

Next is reviewed the popular *Technique Tracking Mode*, the structure of this method is shown in Figure 18 (ASTRöM; HäGGLUND, 1995).

Figure 18 – Structure of PI-AW controller technique Tracking Mode.

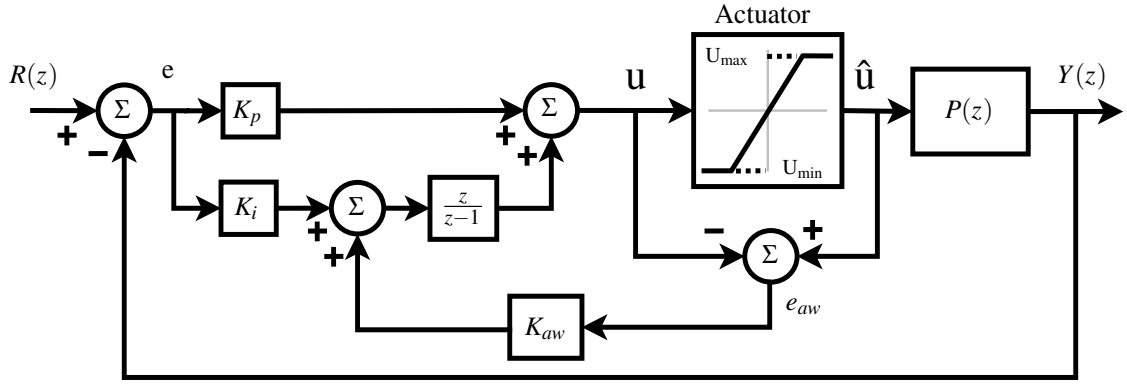

Source: (ASTRöM; HäGGLUND, 1995)

The inclusion of the saturator in control signal is related to the operating limits of the actuators (SHIN; PARK, 2012; SAKAI; ISHIDA, 2016) and it is given by Equation (2.1).

Where the new equation after the saturator (see Equation (2.1)) applied to the plant with Anti-windup is given by:

$$\mathrm{u}(z) = K_p \mathrm{e}(z) + K_i \frac{z}{z-1} \left[\mathrm{e}(z) + K_{aw} \left(\hat{\mathrm{u}}(z) - \mathrm{u}(\mathrm{z})\right)\right] \tag{3.14}$$

The notion of proportional band is useful to understand the Windup effect. The proportional band is defined as the range of process outputs where the controller output is in the linear range. For a PI controller it has (ASTRöM; HäGGLUND, 1995):

$$y_{max} = y_{sp} + \frac{\mathrm{I} - \mathrm{U}_{\max}}{K} \tag{3.15}$$

$$y_{min} = y_{sp} + \frac{\mathrm{I} - \mathrm{U}_{\min}}{K} \tag{3.16}$$

The controller operates in the linear mode, if the predicted output is in the proportional band (Denotes the maximum control error the controller can handle with the available control signal). The control signal saturates when the predicted output is outside the proportional band. Notice that the proportional band can be shifted by changing the integral term.

The idea of *Track Mode Technique* is: when the output of actuator is saturated $\hat{\mathrm{u}} = \mathrm{U}_{\max}$ or $\hat{\mathrm{u}} = \mathrm{U}_{\min}$, the integral term is calculated another time in a way that its value stays

inside the linear limit of the actuator. In Figure 18, the system presents an additional feedback-loop. The difference between input and output of the actuator constitutes an error e_{aw} that is added to the input of integrator with a gain of ($K_{aw} = 1/T_{aw}$). When the saturation does not exist, the error e_{aw} is null and the controller is operating in the linear region. In other words, the signal u is not saturated. If there is saturation, e_{aw} is different from zero. The time taken by the integrator input to tend to zero is determined by the gain $1/T_{aw}$, where T_{aw} can be interpreted as the time constant that determines how fast the input of the integrator becomes zero. The selection of small values for T_{aw} can be advantageous. However, a small value choice for T_{aw} should be carefully made, especially for systems with derivative action. What may happen is that the measurement noise can take the output of the controller into saturation state, resulting in a fast actuation of the anti-windup loop and making the input of the controller undesirably zero. In practice, an empiric selection of rule suggests $T_{aw} = \sqrt{T_i}$ or $T_{aw} = T_i$ (ASTRöM; HäGGLUND, 1995; HU; LIN, 2001b).

3.2 Model Predictive Control

Model predictive control (MPC) has been a control strategy widely used and investigated in both industry (in applications in the process, chemical, food processing and paper industries) and academia. The main reason of this control strategy came by his great capacity of work with all kinds of processes and primarily by handling processes constraints implicitly. For the majority of cases, the optimization problem formulated in MPC is given for a single objective problem. Some of the most popular MPC algorithms well accepted in industry are the Dynamic Matrix Control (DMC) (CAMACHO; BORDONS, 1999), Model Algorithmic Control (MAC) (ALLGöWER; ZHENG, 2000), Predictive Functional Control (PFC) (ALLGöWER; ZHENG, 2000), Extended Prediction Self Adaptive Control (EPSAC), Extended Horizon Adaptive Control (EHAC) and Generalized Predictive Control (GPC) (CAMACHO; BORDONS, 1999). In this work, among these number of MPC algorithms, GPC is particularly studied to its importance and popularity.

3.2.1 GPC Controller

The GPC method was proposed by (CLARKE *et al.*, 1987) and has become one of the most popular of MPC methods both in industry and academia. It has been successfully im-

plemented in many industrial applications, showing good performance and robustness. The basic idea of GPC is to compute a sequence of future control signals in such a way that it minimizes a multistage cost function defined over a prediction horizon, given by (CAMACHO; BORDONS, 1999):

$$J_{(N_1,N_2,N_u)} = \sum_{j=N_1}^{N_2} \delta(j)[y(t+j|t) - w(t+j)]^2 + \sum_{j=0}^{N_u-1} \lambda(j)[\Delta u(t+j-1)]^2. \tag{3.17}$$

where N_1 and N_2 are the prediction horizons minimum and maximum respectively, N_u is the control horizon, λ and δ are positive weighting matrices, $w(t+j)$ is the future reference trajectory, Δu is the incremental control action $\Delta = 1 - q^{-1}$, with q^{-1} represents the delay operator, $u(t+j-1)$ is the incremental control and $y(t+j|t)$ is the prediction of output $y(t)$ from the instant t.

The GPC algorithm is based on Controlled *Auto Regressive Integrated Moving Average* (CARIMA) model and can be described after linearization considering the operation around a particular set point of a SISO (Single Input, Single Output) plant, then can be described as (CAMACHO; BORDONS, 1999):

$$A(q^{-1})y(t) = q^{-d}B(q^{-1})u(t-1) + T(q^{-1})\frac{e(t)}{\Delta}, \tag{3.18}$$

where $A(q^{-1})$, $B(q^{-1})$, $T(q^{-1})$ are polynomials in the form of delay given by q^{-1}:

$$A(q^{-1}) = 1 + a_1 q^{-1} + a_2 q^{-2} + \cdots + a_{n_a} q^{-n_a}, \tag{3.19}$$

$$B(q^{-1}) = b_0 + b_1 q^{-1} + b_2 q^{-2} + \cdots + b_{n_b} q^{-n_b}, \tag{3.20}$$

$$T(q^{-1}) = 1 + t_1 q^{-1} + t_2 q^{-2} + \cdots + t_{n_T} q^{-n_T}, \tag{3.21}$$

where $y(t)$ is the output of the system at instant t, $u(t)$ is the input of system at instant t, Δ is the integration operator given by $\Delta = 1 - q^{-1}$, q^{-d} describes the natural delay, in multiples of the sampling period, $e(t)$ is a white noise of zero mean and variance σ^2, the indices n_a, n_b and n_T are the degrees of the polynomials $A(q^{-1})$, $B(q^{-1})$ and $T(q^{-1})$ respectively (CAMACHO; BORDONS, 1999; MEGíAS *et al.*, 1997).

The last term of the Equation (3.18) can be written as:

$$n(t+j) = \frac{T(q^{-1})}{\Delta}e(t), \tag{3.22}$$

where $T(q^{-1})$ is a polynomial, Δ is $(1-q^{-1})$ and $e(t)$ is the prediction error. A necessary condition is that the degree of polynomials $T(q^{-1})$ and $A(q^{-1})$, comply $n_T \leq n_a + 1$.

Second (MCINTOSH S. L. SHAH, 1991) and (LAMBERT, 1987), the polynomial $T(q^{-1})$ is of second order, which sufficient for to constitute a low pass filter. Thus by the characteristics of study plants in this thesis was chosen the T-polynomial as:

$$T(q^{-1}) = \left(1-\alpha q^{-1}\right)\left(1-\alpha q^{-1}\right). \tag{3.23}$$

The tuning variable for disturbance and noise rejection depends of pole α, which to stay between $0 \leq \alpha \leq 1$, because the cutoff frequency is $F_c = \frac{-ln(\alpha)}{T_s}$ (BORDIGNON, 2016).

The calculation of predictions is recursively performed from the *Diophantine* equation, then the Equation (3.18) turns to:

$$\Delta A(q^{-1})y(t) = q^{-d}B(q^{-1})\Delta u(t-1) + T(q^{-1})e(t). \tag{3.24}$$

In order to perform output predictions $j-$steps ahead, one must write the above Equation (3.24) as follows:

$$\widetilde{A}(q^{-1})y(t+j) = B(q^{-1})\Delta u(t+j-1) + T(q^{-1})e(t+j), \tag{3.25}$$

where $\Delta A = \widetilde{A}(q^{-1})$ whose grade is n_a+1, then:

$$\widetilde{A}(q^{-1}) = 1 + \tilde{a}_1 q^{-1} + \tilde{a}_2 q^{-2} + \cdots + \tilde{a}_{n_a+1} q^{-(n_a+1)}, \tag{3.26}$$

The term related to the noise in Equation (3.25) is then decomposed by applying Diophantine Equation (3.27) leading to:

$$\frac{T(q^{-1})}{\tilde{A}(q^{-1})} = E_j(q^{-1}) + \frac{q^{-j}F_j(q^{-1})}{\tilde{A}(q^{-1})}. \tag{3.27}$$

Which may be rearranged as:

$$T(q^{-1}) = \widetilde{A}(q^{-1})E_j(q^{-1}) + q^{-j}F_j(q^{-1}); \tag{3.28}$$

$$E_j(q^{-1})\tilde{A}(q^{-1}) = T(q^{-1}) - q^{-j}F_j(q^{-1}). \tag{3.29}$$

where $E_j(q^{-1})$ and $F_j(q^{-1})$ are uniquely defined polynomials whose degrees are $(j-1)$ and equal for $\widetilde{A}(q^{-1})$ respectively. Such polynomials can be obtained by successive divisions of

$T(q^{-1})$ by $\widetilde{A}(q^{-1})$, until the rest of the division can be factorized as $q^{-j}F_j(q^{-1})$. The quotient of the division is the polynomial $E_j(q^{-1})$. If both members of Equation (3.25) are multiplied by $E_j(q^{-1})$.

$$E_j(q^{-1})\Delta A(q^{-1})y(t+j) = E_j(q^{-1})B(q^{-1})\Delta u(t+j-1) + E_j(q^{-1})T(q^{-1})e(t+j), \tag{3.30}$$

Substituting in Equation (3.29) as:

$$\begin{aligned}
[T(q^{-1}) - q^{-j}F_j(q^{-1})]\widetilde{A}y(t+j) &= E_j(q^{-1})B(q^{-1})\Delta u(t+j-1) + E_j(q^{-1})T(q^{-1})e(t+j),\\
T(q^{-1})y(t+j) - q^{-j}y(t+j)F_j(q^{-1}) &= E_j(q^{-1})B(q^{-1})\Delta u(t+j-1) + E_j(q^{-1})T(q^{-1})e(t+j),\\
T(q^{-1})y(t+j) - y(t)F_j(q^{-1}) &= E_j(q^{-1})B(q^{-1})\Delta u(t+j-1) + E_j(q^{-1})T(q^{-1})e(t+j),\\
y(t+j) &= \frac{F_j(q^{-1})}{T(q^{-1})}y(t) + \frac{E_j(q^{-1})B(q^{-1})}{T(q^{-1})}\Delta u(t+j-1) + E_j(q^{-1})e(t+j),
\end{aligned} \tag{3.31}$$

Since the degree of $E_j(q^{-1})$ equal $(j-1)$, then all the terms of the noise are in the future, therefore the optimal prediction is obtained by changing $e(t+j)$ by its expected value (zero), thus:

$$y(t+j|t) = \frac{F_j(q^{-1})}{T(q^{-1})}y(t) + \frac{E_j(q^{-1})B(q^{-1})}{T(q^{-1})}\Delta u(t+j-1), \tag{3.32}$$

From Equation (3.32) the past control inputs can be separated from the present and future control by solving a new Diophantine equation as:

$$\frac{E_j(q^{-1})B(q^{-1})}{T(q^{-1})} = H_j(q^{-1}) + q^{-j}M(q^{-1}). \tag{3.33}$$

which can be written as:

$$E_j(q^{-1})B(z^{-1}) = H_j(z^{-1})T(q^{-1}) + q^{-j}T(q^{-1})M(q^{-1}), \tag{3.34}$$

$$I_j(q^{-1}) = T(q^{-1})M(q^{-1}), \tag{3.35}$$

$$E_j(q^{-1})B(q^{-1}) = H_j(q^{-1})T(q^{-1}) + q^{-j}I_j(q^{-1}), \tag{3.36}$$

where H_j with degree of $j-1$ and it is a matrix of response to the unit step of $P(q^{-1})$. Using Equations (3.36) and (3.33) the output predictions can be rewritten as:

$$y(t+j|t) = H_j(q^{-1})\Delta u(t-1+j|t) + F_j(q^{-1})\frac{y(t)}{T(q^{-1})} + \frac{I_j(q^{-1})}{T(q^{-1})}\Delta u(t-1), \tag{3.37}$$

Since the point of view the controller implementation , an analytical solution with low computational cost is important since the implementation will be carried out in the DSP. Thus in this sense, this work addresses the special case where $N_u = 1$, $N_1 = 0$, $N_2 = N$ and $\lambda = 0$. Interactively solving Equation (3.37) is obtained:

$$\begin{aligned}
y(t+1|t) &= H_1(q^{-1})\Delta u(t-1+1|t) + F_1(q^{-1})\frac{y(t)}{T(q^{-1})} + \frac{I_1(q^{-1})}{T(q^{-1})}\Delta u(t-1),\\
y(t+2|t) &= H_2(q^{-1})\Delta u(t-1+2|t) + F_2(q^{-1})\frac{y(t)}{T(q^{-1})} + \frac{I_2(q^{-1})}{T(q^{-1})}\Delta u(t-1),\\
&\vdots\\
y(t+N|t) &= H_N(q^{-1})\Delta u(t-1+N|t) + F_N(q^{-1})\frac{y(t)}{T(q^{-1})} + \frac{I_N(q^{-1})}{T(q^{-1})}\Delta u(t-1),
\end{aligned} \tag{3.38}$$

Can be written in vectorial form:

$$\mathbf{y} = \mathbf{G}\Delta\mathbf{u} + \mathbf{F}(q^{-1})\frac{y(t)}{T(q^{-1})} + \mathbf{I}(q^{-1})\frac{\Delta u(t-1)}{T(q^{-1})}, \tag{3.39}$$

where the variables $y(t)$ and $\Delta u(t-1)$ are filtered by $T(q^{-1})$ (CAMACHO; BORDONS, 1999).

$\mathbf{G}$ is a matrix based on the coefficients of $H_j(q^{-1})$, of the form:

$$\mathbf{G} = [h_1 \quad h_2 \quad \cdots \quad h_N]^{Tr}, \tag{3.40}$$

Tr is transposed of the vector or matrix.

$$\mathbf{f} = \mathbf{F}(q^{-1})\frac{y(t)}{T(q^{-1})} + \mathbf{I}(q^{-1})\frac{\Delta u(t-1)}{T(q^{-1})}, \tag{3.41}$$

$\mathbf{f}$ is the free response, so:

$$\mathbf{y} = \mathbf{f} + \mathbf{G}\Delta\mathbf{u} \tag{3.42}$$

Therefore, the Equation (3.17) can be written as:

$$J = (\mathbf{G}\Delta\mathbf{u} + \mathbf{f} - \mathbf{w})^{Tr}(\mathbf{G}\Delta\mathbf{u} + \mathbf{f} - \mathbf{w}) + \lambda\Delta\mathbf{u}^{Tr}\Delta\mathbf{u}, \tag{3.43}$$

developing Equation (3.43) as:

$$\begin{aligned}
J &= (\mathbf{G}\Delta\mathbf{u})^{Tr}\mathbf{G}\Delta\mathbf{u} + (\mathbf{G}\Delta\mathbf{u})^{Tr}(\mathbf{f}-\mathbf{w}) + (\mathbf{f}-\mathbf{w})^{Tr}\mathbf{G}\Delta\mathbf{u} + (\mathbf{f}-\mathbf{w})^{Tr}(\mathbf{f}-\mathbf{w}) + \lambda\Delta\mathbf{u}^{Tr}\Delta\mathbf{u},\\
J &= [(\mathbf{G}\Delta\mathbf{u})^{Tr}\mathbf{G} + (\mathbf{f}-\mathbf{w})^{Tr}\mathbf{G} + \lambda\Delta\mathbf{u}^{Tr}]\Delta\mathbf{u} + (\mathbf{G}\Delta\mathbf{u})^{Tr}(\mathbf{f}-\mathbf{w}) + (\mathbf{f}-\mathbf{w})^{Tr}(\mathbf{f}-\mathbf{w}),\\
J &= [\Delta\mathbf{u}^{Tr}\mathbf{G}^{Tr}\mathbf{G} + (\mathbf{f}-\mathbf{w})^{Tr}\mathbf{G} + \lambda\Delta\mathbf{u}^{Tr}]\Delta\mathbf{u} + \Delta\mathbf{u}^{Tr}\mathbf{G}^{Tr}(\mathbf{f}-\mathbf{w}) + (\mathbf{f}-\mathbf{w})^{Tr}(\mathbf{f}-\mathbf{w}),\\
J &= \Delta\mathbf{u}^{Tr}(\mathbf{G}^{Tr}\mathbf{G} + \lambda\mathbf{I})\Delta\mathbf{u} + 2(\mathbf{f}-\mathbf{w})^{Tr}\mathbf{G}\Delta\mathbf{u} + (\mathbf{f}-\mathbf{w})^{Tr}(\mathbf{f}-\mathbf{w}).
\end{aligned} \tag{3.44}$$

The parameters are:

$$\mathbf{H} = 2(\mathbf{G}^{Tr}\mathbf{G} + \lambda\mathbf{I}), \tag{3.45}$$

$$\mathbf{b}^{Tr} = 2(\mathbf{f} - \mathrm{w})^{Tr}\mathbf{G}, \tag{3.46}$$

$$\mathbf{f_0} = (\mathbf{f} - \mathbf{w})^{Tr}(\mathbf{f} - \mathbf{w}). \tag{3.47}$$

Thus it obtains the following cost function to minimize of Equation (3.44) as:

$$J = \frac{1}{2}\Delta\mathbf{u}^{Tr}\mathbf{H}\Delta\mathbf{u} + \mathbf{b}^{Tr}\Delta\mathbf{u} + \mathbf{f}_0, \tag{3.48}$$

The solution to this problem optimization is a crucial step in the algorithms based on GPC. Numerical complexity depends on the model characteristics in terms of linearity, constraints, number of controlled and manipulated variables, etc., and then it has two cases:

3.2.1.1 Unconstrained optimization

In a non-restricted case ,i.e., without saturation the controller which minimizes the cost function according to Camacho (CAMACHO; BORDONS, 1999) is analytically calculated as:

Note: It is known that the gradient of a function of type: $\frac{\partial \mathbf{g}}{\partial \mathbf{x}} = (\mathbf{A} + \mathbf{A}^{Tr})\mathbf{x} + b.$

$$\frac{\partial J}{\partial u} = \frac{1}{2}\left(\mathbf{H} - \mathbf{H}^{Tr}\right)\Delta u + \mathbf{b}. \tag{3.49}$$

As $\mathbf{H}$ is symmetric , therefore:

$$\Delta\mathbf{u} = -\mathbf{H}^{-1}\mathbf{b}. \tag{3.50}$$

When it is used a sliding horizon strategy, the control signal applied to process is represented for the first element of second vector is given by:

$$\Delta\mathbf{u} = (\mathbf{G}^{Tr}\mathbf{G} + \lambda\mathbf{I})^{-1}\mathbf{G}^{Tr}(\mathbf{w} - \mathbf{f}). \tag{3.51}$$

As in practice only the current control action is applied, it has:

$$\Delta u = \mathbf{K}(\mathbf{w} - \mathbf{f}), \tag{3.52}$$

where $\mathbf{K}$ is equal to the first line of $(\mathbf{G}^{Tr}\mathbf{G}+\lambda\mathbf{I})^{-1}\mathbf{G}^{Tr}$ with dimension 1xN, $\mathbf{G}$ is NxN_u constant matrix based on the coefficients $H_j(q^{-1})$ and $\mathbf{w}$ is a vector of the future reference (SIMKOFF *et al.*, 2017).

The controller implementation standpoint, an analytical solution with low computational cost is important. Thus, this work is concerned a $N = N_u = 1$, and $\lambda = 0$, which represents the best trade off between computational cost and closed-loop performance (SILVA *et al.*, 2013).

For the application it is proceeded to synthesize this digital controller in the structure known as **RST**, which allows the study of aspects related stability and robustness for linear controllers. Then the equation of a digital controller in the **RST** form is:

$$\mathrm{u(t)} = \frac{1}{\Delta\mathbf{R}(q^{-1})}\left[\mathbf{T}(q^{-1})r(t) - \mathbf{S}(q^{-1})y(t)\right], \tag{3.53}$$

of the Equation (3.52):

$$\Delta u = \sum_{i=1}^{N} K_i\left[w(t) - f(t)\right]. \tag{3.54}$$

Substituting the free answer for its equivalence given by Equation (3.41), it has that:

$$\Delta\mathrm{u} = \sum_{i=1}^{N} K_i w(t) - \sum_{i=1}^{N} K_i F_i \frac{y(t)}{T(q^{-1})} - \sum_{i=1}^{N} K_i I_i \frac{\Delta u(t-1)}{T(q^{-1})}, \tag{3.55}$$

$$\left[T(q^{-1}) + q^{-1}\sum_{i=1}^{N} K_i I_i\right]\Delta\mathrm{u(t)} = T(q^{-1})\sum_{i=1}^{N} K_i w(t) - \sum_{i=1}^{N} K_i F_i y(t), \tag{3.56}$$

$$\mathrm{u(t)} = \frac{1}{\Delta\left[T(q^{-1}) + q^{-1}\sum_{i=1}^{N} K_i I_i\right]}\left[T(q^{-1})\sum_{i=1}^{N} K_i w(t) - \sum_{i=1}^{N} K_i F_i y(t)\right]. \tag{3.57}$$

Through some manipulations, Equation (3.53) can be written in the **RST** form (ALMEIDA *et al.*, 2014):

$$r(t) = w(t+i), \tag{3.58}$$

is the setpoint and:

$$\mathbf{T}(q^{-1}) = T(q^{-1})\sum_{i=1}^{N} K_i, \tag{3.59}$$

$$\mathbf{S}(q^{-1}) = \sum_{i=1}^{N} K_i F_i(q^{-1}), \tag{3.60}$$

$$\mathbf{R}(q^{-1}) = T(q^{-1}) + q^{-1}\sum_{i=1}^{N} K_i I_i(q^{-1}). \tag{3.61}$$

The controller proposed by (ALMEIDA *et al.*, 2014) is designed to filter the control signal. Besides a tuning the controller is based on a single parameter α that allows good trade-offs among noise attenuation of the control signal, disturbance rejection and system robustness during operation, called GPC based control (GPCBC). Thus, the control polynomials **R**, **S**, and **T** are given by (DIAS, 2016):

$$\mathbf{T}(q^{-1}) = \frac{(1-\alpha)T(q^{-1})}{b_0}, \tag{3.62}$$

$$\mathbf{R}(q^{-1}) = 1 - \alpha t_2 q^{-1}, \tag{3.63}$$

$$\mathbf{S}(q^{-1}) = \frac{2-\alpha+t_1+\alpha t_2-(1+\alpha t_1+(2\alpha-1)t_2)q^{-1}}{b_0}, \tag{3.64}$$

$$\alpha = 1 - \frac{1+2+3+\cdots+N}{1+2^2+3^2+\cdots+N^2}. \tag{3.65}$$

It is observed that the polynomials **R**, **S**, **T**, contain the alpha parameter which depends on N. From Equation (3.65) it is readily seen that $\alpha = 0$ if $N = 0$ and $\alpha \to 1$ as $N \to \infty$. Therefore, for this approach prediction horizon N may be used as a setting parameter (DIAS *et al.*, 2016). From hereafter it is applied α as an adjustment parameter in this work.

Figure 19 – Classical RST structure applied to SRM speed control.

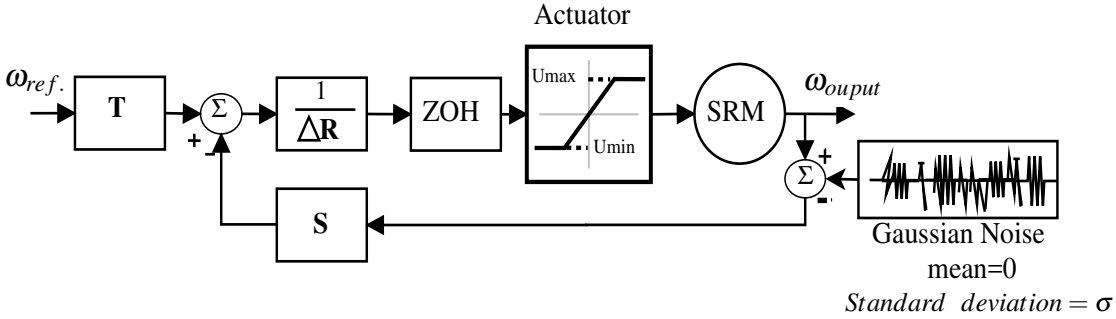

Source: Author.

The analysis of this diagram lead to the following transfer functions relating reference $\omega_{ref.} = R(z)$ with output $\omega_{ouput} = Y(z)$, alongside with input disturbance $M(z)$, and output Gaussian noise $N(z)$, by the equations:

$$H_{Y-R}(z) = \frac{Y(z)}{R(z)} = \frac{\mathbf{T}(z)\mathbf{G}(z)}{\Delta\mathbf{R}(z) + \mathbf{S}(z)\mathbf{G}(z)}, \tag{3.66}$$

$$H_{Y-M}(z) = \frac{Y(z)}{M(z)} = \frac{\Delta\mathbf{R}(z)\mathbf{G}(z)}{\Delta\mathbf{R}(z)+\mathbf{S}(z)\mathbf{G}(z)}, \tag{3.67}$$

$$H_{u-n}(z) = \frac{u(z)}{n(z)} = \frac{-\mathbf{S}(z)}{\Delta\mathbf{R}(z)+\mathbf{S}(z)\mathbf{G}(z)}, \tag{3.68}$$

$$H_{Y-N}(z) = \frac{Y(z)}{N(z)} = \frac{-\mathbf{S}(z)\mathbf{G}(z)}{\Delta\mathbf{R}(z)+\mathbf{S}(z)\mathbf{G}(z)}. \tag{3.69}$$

3.2.1.2 Constrained optimization

The main advantages of the GPC predictive control is its ability to incorporate constraints in the design of the controller (BANERJEE *et al.*, 2017), by taking numerical optimization, instead of analytical one described in the previous section.

Constraints may be related to limitations on the maximum and minimum magnitudes of the control action described by:

$$\mathrm{U_{min}} \leq u(t+j|t) \leq \mathrm{U_{max}} \quad , \quad \forall j = 0,\ldots,N_u-1, \tag{3.70}$$

In addition, one may consider limitations on the speed of variation of control action:

$$\Delta u_{min} \leq \Delta u(t+j|t) \leq \Delta u_{max} \quad , \quad \forall j = 0,\ldots,N_u-1, \tag{3.71}$$

And also limitations on the maximum and minimum quantities allowed for the outputs:

$$y_{min} \leq y(t+j|t) \leq y_{max} \quad , \quad \forall j = 1,\ldots,N_2, \tag{3.72}$$

In this work the only restriction to be a consideration is the saturation for the control signal that relates a real process with restrictions (HUANG *et al.*, 2017).

Thus now is form a matrix as:

$$\mathbf{1}(\mathrm{U_{min}} - u(t-j)) \leq \mathrm{Qu} \leq \mathbf{1}\mathrm{U_{max}} - u(t-j) \quad , \forall t, \tag{3.73}$$

where $\mathbf{1}$ is a unitary matrix $N_u x 1$ and $\mathbf{Q}$ is a lower triangular matrix $N_u x N_u$ with unitary elements. Inequality Equation (3.73) indicates that, at all sampling instants belonging to the

interval $[t, t+N_u-1]$, the restriction given by Equation (3.73) is satisfied if it is used in solving the optimization problem. Rewriting Equation (3.70) in a more compact form.

$$\mathbf{Pu} \leq \mathbf{c}, \tag{3.74}$$

where:

$$\mathbf{P} = \begin{bmatrix} \mathbf{Q} \\ -\mathbf{Q} \end{bmatrix}; \mathbf{c} = \begin{bmatrix} \mathbf{1}(\mathrm{U_{min}} - u(t-1)) \\ -\mathbf{1}\mathrm{U_{max}} - u(t-1) \end{bmatrix}. \tag{3.75}$$

Therefore, the optimization problem to be solved, is given as:

$$Minimize: \qquad J = \frac{1}{2}\Delta\mathbf{u}^{Tr}\mathbf{H}\Delta\mathbf{u} + \mathbf{b}^{Tr}\Delta\mathbf{u} + \mathbf{f}_0, \tag{3.76}$$

$$subject \qquad to: \mathbf{Pu} \leq \mathbf{c}. \tag{3.77}$$

The literature presents several numerical methods to solve the optimization problem with some described in (CAMACHO; BORDONS, 1999). A disadvantage in solving the optimization problem is the computational effort involved, which may require time not available in certain practical cases.

The problem of cost function optimization J with linear constraints (saturator) is usually known as a Quadratic Programming (QP) problem (HUANG *et al.*, 2017). Such solution is based on convex analysis (minimization problem) of the control signal u on a convex set, resolved numerically (CAMACHO; BORDONS, 1999). MATLAB command *quadprog* is a well known and efficient implementation to solve Equation (3.76).

$$\mathbf{u} = quadprog(H; b; P; c) \tag{3.78}$$

Figure 20, future reference (Ref) is subtracted from the future predicted outputs by the model (Ym). This difference of error (e) is introduced in the optimizer, that calculates an optimal output (u) (taking into account the cost function), also considering the restriction of the saturation (U_{max}, U_{min}) and then it is introduced into the process (Plant). After the process control updates the readings of plant (with Gaussian noise) and the future control signal, these new values are introduced to the plant model, where it repeats the calculation of future predicted outputs for the new sampling period.

Figure 20 – GPC-T controller with constrained

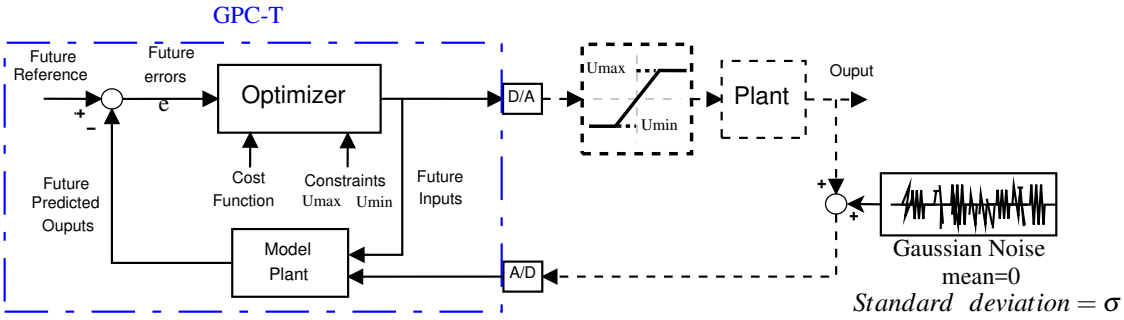

Source: Author.

3.3 Performance Indices

To evaluate the dynamic behavior of the control systems and to compare the goodness of the tuning methods studied in this work, it has been chosen the following performance indices (DORF; BISHOP, 2011):

– Integrated Absolute Error (IAE)

The IAE provides the area under the error curve, which represents the amount of material out of specification, energy lost or other undesired characteristic. The IAE is given by the following equation:

$$IAE = \int_0^\infty |e(t)|dt, \tag{3.79}$$

where $e(t) = r(t) - y(t)$, $r(t)$ is the process reference and $y(t)$ and is the output of process. If $IAE \to 0$, then $y(t) \to r(t) \forall t$ if the control were perfect.

Although the magnitude of the IAE is an indication of the goodness of the tuning method with respect to error is more useful, for comparison effects with respect to other tuning methods, its relative value with respect to the value of the IAE that would be obtained if the parameters of the controller were optimal with regard to that criterion (OGATA, 1997).

– Total Variation (TV)

the Integral of absolute values of the error TV is also a performance criterion for closed-loop response, but in contrast to the IAE, the objective for TV is to measure the total variation in the controller output signal, u.

$$TV = \int_0^\infty \left| \frac{d(u(t))}{dt} \right| dt \tag{3.80}$$

or

$$TV = \sum_{i=0}^{\infty} |u_{i+1} - u_i| \tag{3.81}$$

where u_i and u_{i+1} are the signal of present and future control, respectively (ROJAS, 2011). The desired value TV, as well as IAE is to have low values.

– Steady State Error (e_{ss})

The steady-state error is that error that remains after of what finish the transient. In which the signals of the system remain constant, while not having an external signal. This error can be calculated by the final value theorem, the limit of a function in the time domain, when time tends to infinity can be found through the product limit of the Laplace transform of the function by the Laplace variable, when it tends to zero (OGATA, 1997) .

$$e_{ss}(t) = \lim_{t\to\infty} e(t) \Rightarrow e_{ss} = \lim_{s\to 0} sE(s) \qquad \%e_{ss} = \bar{e}_{ss} * 100 \tag{3.82}$$

The desired value $\%e_{ss}$ is zero as ideal, but it is acceptable if it has a value close to zero that to depend of the process.

4 CASE STUDIES

This chapter is divided in two parts, the first one is intended to present comparative analysis for PI-AW and GPC-T controllers in different processes as stable and integrative plants. These plants are considered to be subjected to saturation in control signal and Gaussian noise in the feedback loop, in order to highlight the presence of the NITE phenomenon. In the GPC-T control with structure of the subsection 3.2.1.2 (see Figure 20) , the change parameter α of the T-polynomial do not has a relation direct with noise power is commonly considered as a design parameter. Therefore, for this study α varies according to the values $\alpha = [0,0,24,0,44,0,64,0,84,0,94]$, whose step is for a better appreciation of its evolution with respect to the noise and mitigation of the NITE phenomenon. Finally, validate the comparison with the help of performance indices among the controls studied.

For the second part, as already described, it was used the laboratory prototype in the speed control of an SRM, whose details of the best setup are explained in the proper section of this work. Thus will perform comparative study of SRM speed control between the PI-AW and GPC-T controllers, under the presence of saturation and noise. The NITE phenomenon is investigated for such experimental plant and its respective mitigation by implementing the T-polynomial for the GPC controller under the same range previously selected for α, therefore for the GPC-T controller is applying the equivalent structure **RST** (see subsection 3.2.1.1). Finally, it also validate the comparison by computing performance indices between the controllers.

Figure 21 – Comparison structure of the PI-AW and GPC-T controllers

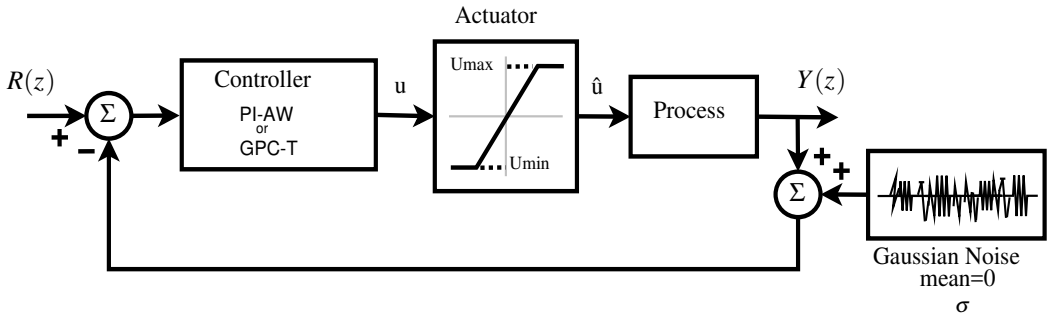

Source: Author.

4.1 Stable process

The case analyzed is a stable open-loop first order process, so the chosen plant is (EUN; S., 2015):

$$P(s) = \frac{1}{3s+1}. \tag{4.1}$$

The setting of the controllers to be compared are:

Firstly, for the PI-AW controller design, it has been considered the parameters $K_p = 5.5$, $K_i = 3.1$, $K_{aw} = 1$, which are obtained through Root Locus Method (see subsection 3.1.2.1) followed by a fine-tuning based on the simulation of the closed loop.

The GPC controller has been tuned with $T_s = 0.1[s], \lambda = 17.1, N = N_u = 100$, in order to exhibit output response similar to the PI-AW in the linear region (without Gaussian noise account)

For both controllers, saturation limits are: $U_{max} = 1$ and $U_{min} = 0$ and Set-point = 0.9. For this analysis, firstly it has been considered a step-like disturbance at time $t = 20\ s$, without Gaussian noise. Results are shown in Figure 22.

Figure 22 – System response with perturbation and without noise

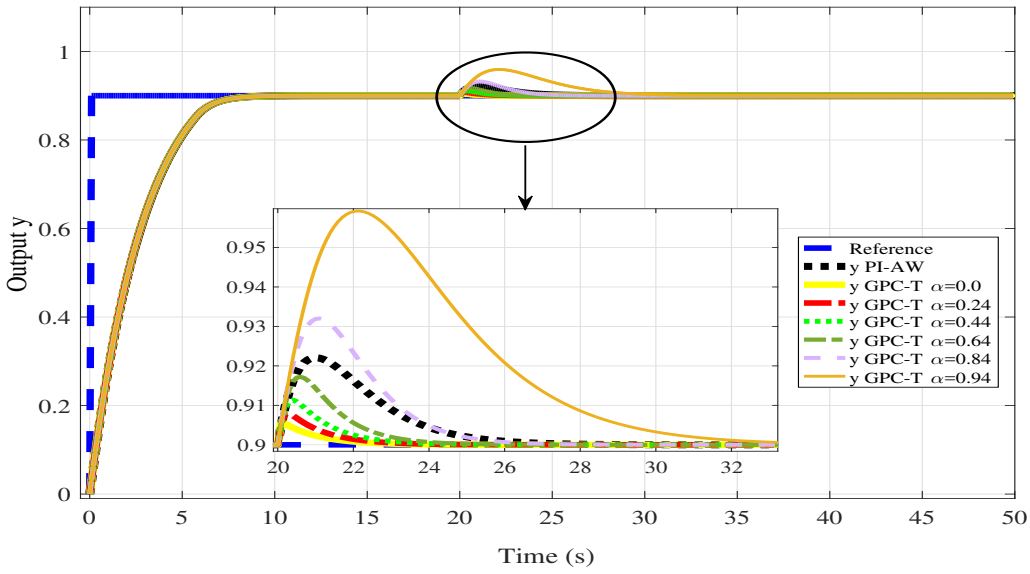

Source: Author.

Figure 23 – Control signal û after saturator

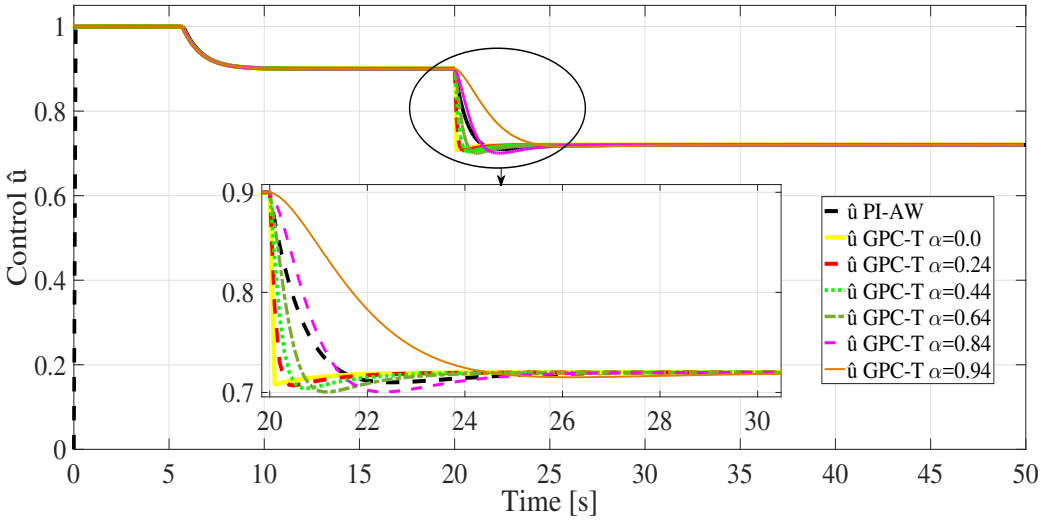

Source: Author.

It is observed from Figure 22 that both controllers obviously have the same response in the transient and settling time, but for the GPC-T control the rejection of the disturbance depends on the T-polynomial and the election of the pole (α). In other words, disturbance rejection can be made faster or slower based on the choice of α. Thus when α is increasing it has slower rejection as $\alpha \to 1$.

From Figure 23 one might note that the control signal stabilizes near the saturation limit, prior to the application of the step disturbance. It is elaborated right away Table 1 of comparison through the performance indices without noise in the feedback loop of PI-AW and GPC-T controllers.

Table 1 – Performance indices without noise for stable plant

Controller	α	**IAE**	**TV**
PI-AW	–	2.0654	1.1000
GPC-T	0.0	2.0041	0.2973
GPC-T	0.24	2.0088	0.2998
GPC-T	0.44	2.0158	0.3051
GPC-T	0.64	2.0312	0.3114
GPC-T	0.84	2.0907	0.3129
GPC-T	0.94	2.3218	0.2886

Source: Author.

Table 1 shows the performance indices of the PI and GPC-T controllers without the presence of noise. Note that IAE is roughly the same for both controllers, when $\alpha = 0$ (see rows 1 and 2 of Table 1). However, GPC-T control exhibit considerably lower control effort as TV index is much smaller. The steady-state error is $\%e_{ss} = 0$ for both controllers, because of

the integral action immersed in these controllers.

Next, Gaussian noise is introduced with noise power $\sigma = 0.1$ (standard deviation) in the feedback loop, whose output response is viewed in Figures 24 and 25.

Figure 24 – System response with Gaussian noise ($\sigma = 0.1$)

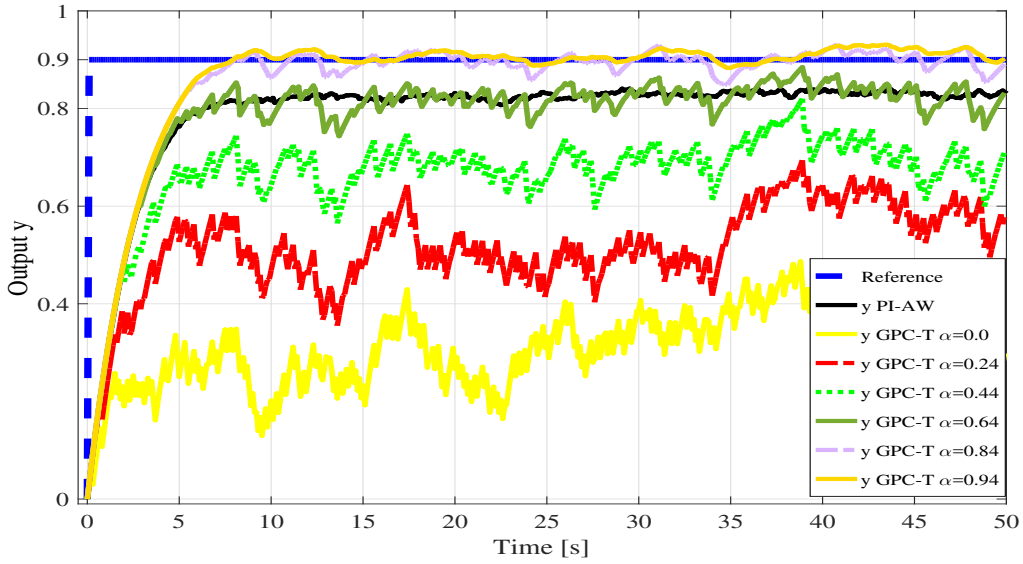

Source: Author.

Figure 25 – Control signal û after saturator

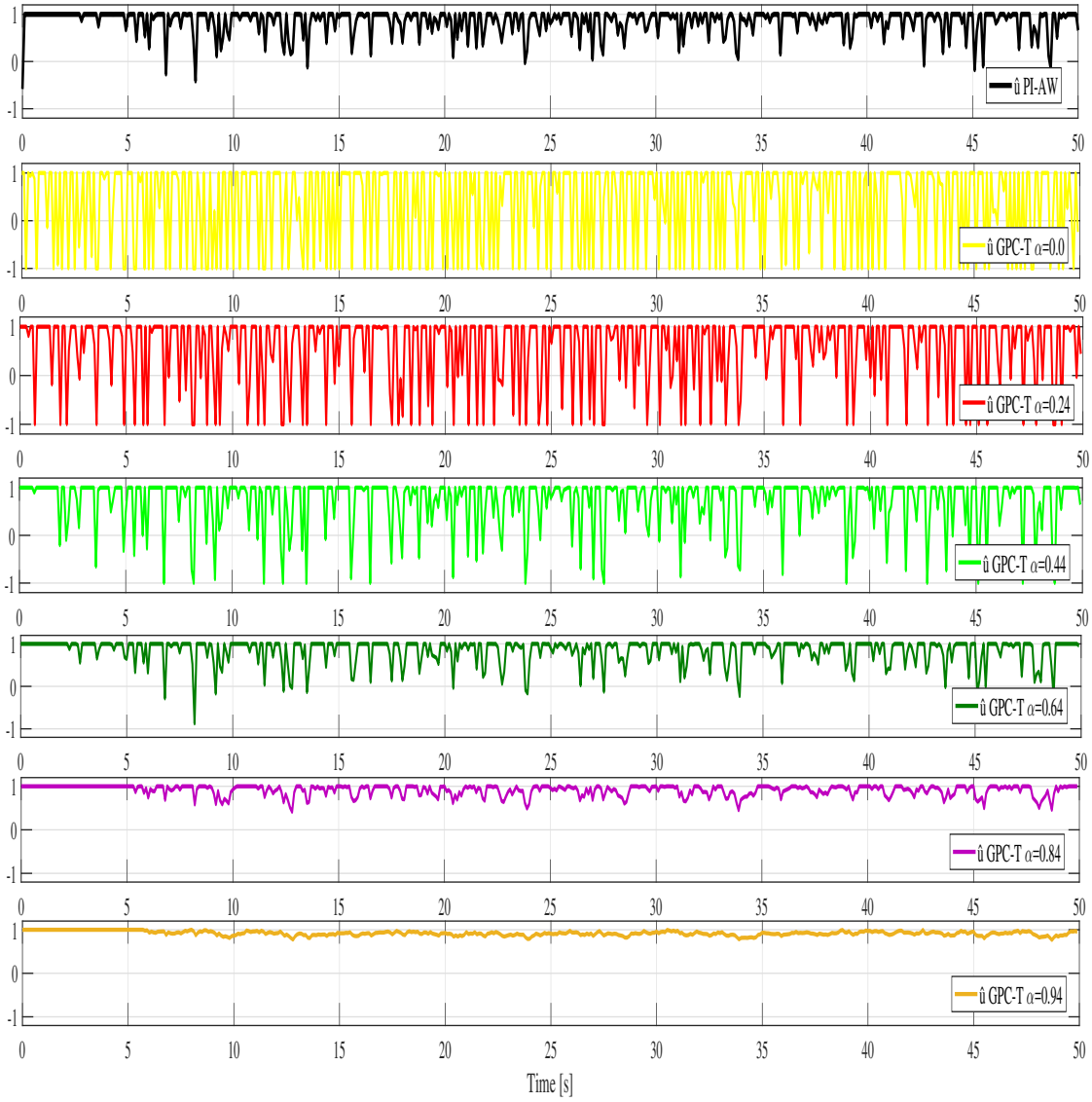

Source: Author.

From Figures 24 and 25 is show that the PI-AW controller cannot follow the reference because of the saturation in control signal, i.e., the NITE phenomenon observed in the article by (EUN; S., 2015). On the other hand, GPC-T controller also has steady-state error with the presence of Gaussian noise in the feedback loop, if $\alpha = 0$ (of T-polynomial), and even greater than that of the PI-AW controller. However, as $\alpha \to 1$, NITE phenomenon is mitigated as noise peaks become smaller falling in the linear region (see Figure 24). Such a result is compliant with the fact that T-polynomial acts as a low-pass filter immersed in the calculation of the controller effort. (MEGíAS *et al.*, 1997; CAMACHO; BORDONS, 1999).

Table 2 presents comparison results of performance indices with noise in the feedback loop for PI-AW and GPC-T controllers.

Table 2 – Performance indices with noise for stable plant

Controller	α	**IAE**	**TV**	$\%e_{ss}$
PI-AW	–	5.7413	115.1141	8.1105
GPC-T	0.0	30.7941	588.8031	61.3032
GPC-T	0.24	20.6534	395.5189	39.1749
GPC-T	0.44	12.5704	238.2452	23.2925
GPC-T	0.64	5.7025	105.9928	8.0017
GPC-T	0.84	2.5615	32.8221	0.1247
GPC-T	0.94	2.4425	8.5627	0.1094

Source: Author.

It concludes from this analysis, that in the presence of noise (see Table 2), the GPC-T controller ($\alpha = 0.0$) has greater steady-state error, in relation to the PI-AW control, by which they have lower performance. By increasing α in GPC-T control until $\alpha = 0.94$, the steady-state error becomes to stay smaller (see Figure 24). Thus, the NITE effect is considerably reduced and its performance is improved relative to the PI-AW.

4.2 Integral process

The analyzed case is a process with integral action so the chosen plant is (HU; LIN, 2001b):

$$P(s) = \frac{180}{s(s+14)}. \tag{4.2}$$

Setting of the controllers to be compared are shows as follows. Firstly, for the PI-AW controller design, it has been considered $K_p = 0.35$, $K_i = 0.5$, $K_{AW} = 3.4$, $T_s = 0.1[s]$, obtained with the application of the Root Locus Method (see subsection 3.1.2.1) along with a tuning based on the simulation of the linear controlled system (without saturation and without Gaussian noise).

The GPC controller has been set with $T_s = 0.1[s]$, $\lambda = 5$, $N = Nu = 150$, in order to get the same response characteristics in the transient and settling time of the PI-AW. Saturation limits are: $U_{max} = 5$ and $U_{min} = -0.3$ and Set-point = 100. For this analysis, a step-like disturbance at time $t = 10\ s$ with $(\%5)$*Reference, without Gaussian noise. Figures 26 and 27 show the results obtained from this simulation.

Figure 26 – System response with perturbation and without noise

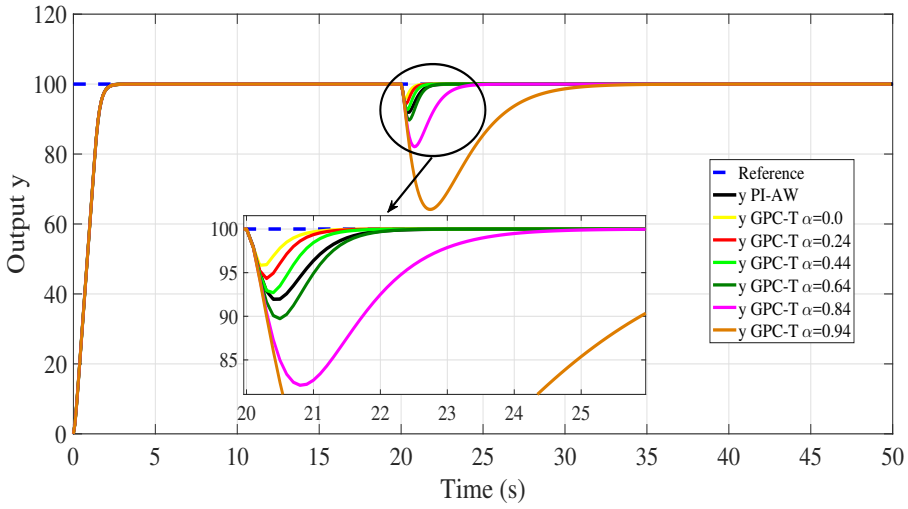

Source: Author.

Figure 27 – Control signal û after saturator

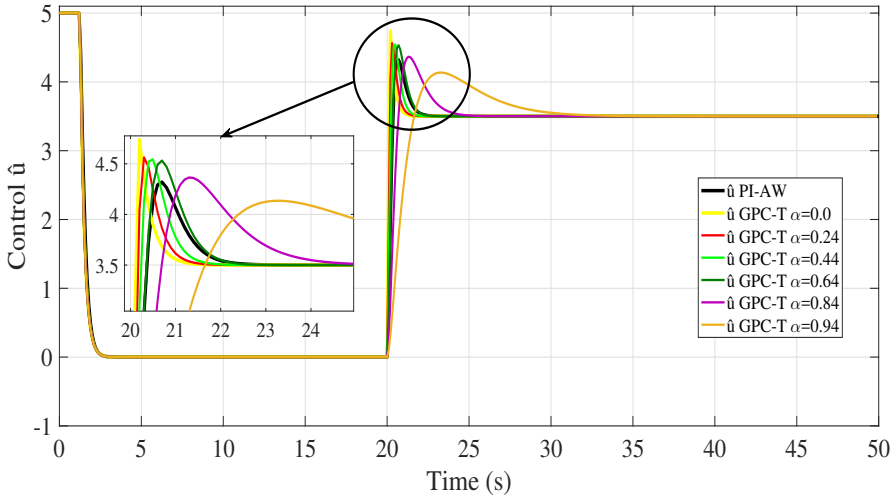

Source: Author.

It is observed from Figure 26 that both controllers have the same response transient. But of the GPC-T control disturbance rejection, already mentioned above, is based on the T-polynomial pole (α), to be fast or slow. So both controllers have a steady-state error $e_{ss} = 0$. It should be noted that the control signal stabilizes near the saturation limit without considering the disturbance.

In order to have a quantitative analysis performance indices are taken in Table 3 for comparison, without noise in the feedback loop for both PI-AW and GPC-T controllers.

Table 3 – Performance indices without noise for integral plant

Controller	α	**IAE**	**TV**
PI-AW	–	94.1187	10.1380
GPC-T	0.0	89.1394	10.9810
GPC-T	0.24	90.1831	10.6266
GPC-T	0.44	91.8975	10.5856
GPC-T	0.64	96.1499	10.5636
GPC-T	0.84	117.7992	10.2297
GPC-T	0.94	245.8966	9.7702

Source: Author.

From Table 3 it can be verified that these controllers have the same characteristics. Then its comparison is feasible and it arrives at the same analysis of the stable plant, in the influence of T-polynomial with respect to the speed of disturbance rejection.

Following, Gaussian noise is introduced in the feedback loop with standard deviation ($\sigma = 5$), leading to output responses seen in Figure 28 and 29.

Figure 28 – System response with Gaussian noise ($\sigma = 5$)

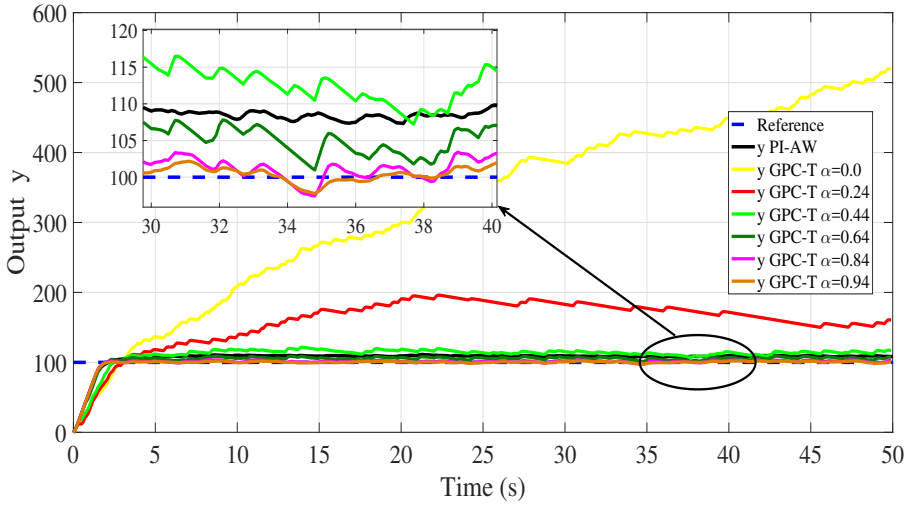

Source: Author.

Figure 29 – Control signal û after saturator

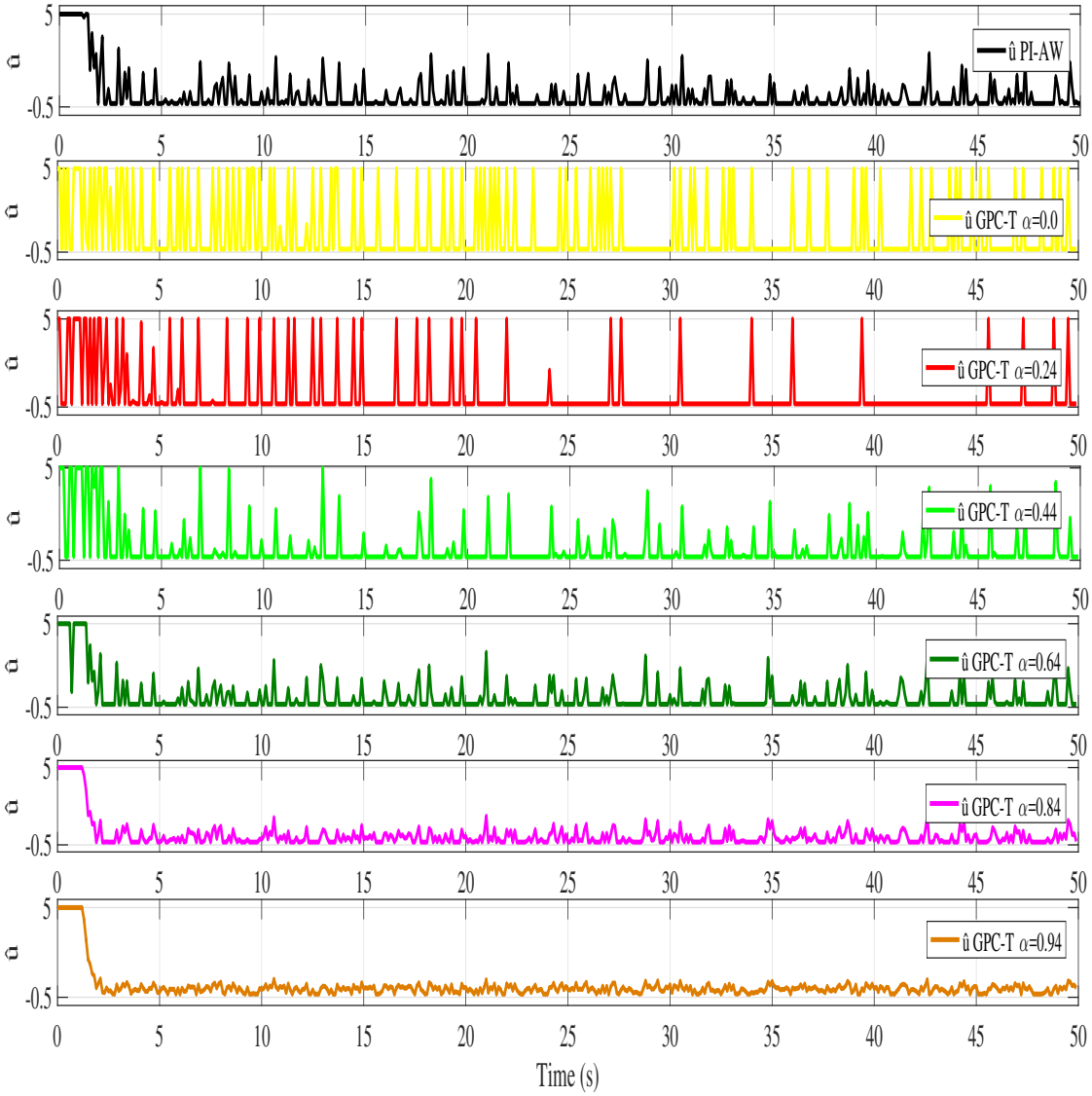

Source: Author.

Table 4 presents comparison analysis of the performance indices, with noise in the feedback loop, for PI-AW and GPC-T controllers.

Table 4 – Performance indices with noise for integral plant

Controller	α	**IAE**(10^4)	**TV**(10^3)	$\%e_{ss}$
PI-AW	–	0.5133	0.2828	8.7994
GPC-T	0.0	1.1646	1.0054	363.3114
GPC-T	0.24	0.3201	0.4630	63.3347
GPC-T	0.44	0.0791	0.3578	12.8111
GPC-T	0.64	0.0364	0.2652	5.4834
GPC-T	0.84	0.0158	0.1788	1.6613
GPC-T	0.94	0.0125	0.1039	0.7479

Source: Author.

Figure 28 shows that both controllers present steady-state error, even for this case where it has been taken an integrative plant. It has to be highlighted that in the control GPC-T ($\alpha = 0$) steady-state error is even greater than that of the PI-AW, i.e., the NITE phenomenon is also present in a plant with internal integral action, which is due to the saturation of the noise peaks (see Figure 29). But when it changes the Pole ($\alpha \neq 0$) from the T-polynomial, it is evident the reduction of the NITE phenomenon Figure 28, because reduce the saturation in signal of control. In Table 4, it is verified that the change of (α) up to 0.94, by the GPC-T control, improves performance on comparison with the PI-AW control, thus reducing considerably the NITE phenomenon.

4.3 Switched Reluctance Motor

The selected plant that presents the characteristics of physical limits in the actuators (saturator) and noise in control loop feedback is the Switched Reluctance Motor (SRM), which has different applications (RAHMAN *et al.*, 2000; KRISHNAN, 2001; TURSINI *et al.*, 2016):

- Aerospace requires auxiliary motors with great fault tolerance, small size and high temperature of work.
- Electric Vehicle Sector, allows the reduction of CO_2 emissions to the atmosphere, high efficiency, ability to work as a generator and return power to the battery.
- Sector of generation, research, development and manufacture of generators coupled to vehicles. For example the turbo-generator.
- Sector of the machine tool, in this case the motor SRM combines the little inertia and high torque capacity, which together with the control of speed and position can be used in machining applications.

A specific example is that at the 2013 Geneva Motor Show, Land Rover unveiled a range of new electric Defender vehicles which are directly powered by an electric motor and drive system developed and built by Nidec SR Drives Ltd (INFINEON, 2017).

In the electric research vehicles, the standard diesel engine and gearbox of the Land Rover 110 Defender has been replaced by an SR Drive® 70 *kW* (94 bhp) switched reluctance (SR) electric motor, twinned with a 300-volt lithium-ion battery with a capacity of 27 *kWh*, giving a range of more than 50 *miles*. It has a top speed of 70 *mph* and, in typical low speed off-road use (4x4), can run for up to eight hours before recharging (INFINEON, 2017).

Figure 30 – New Land Rover 2013 all-electric with motor SRM 4*x*4

Source: <http://www.srdrives.com/land-rover.shtml>

Figure 31 – Testing bench of the SRM engine with 330 N.m. of maximum torque

Source: <http://www.srdrives.com/land-rover.shtml>

A prototype of this machine is available in Electrical Engineering Department of Federal University of Ceará. It applies a Texas Instruments DSP (TMS320F28335) for switch the power converter.

4.3.1 Description of the test prototype

This subsection is dedicated to describe the characteristics and basic operation principle of the SRM. In addition, it is presented a brief characterization of the activation of the test prototype along with specific characterization of SRM 12/8 used in this work.

4.3.1.1 Physical principle of operation SRM

Physical principle of operation SRM is based on the variation of reluctance of the rotor magnetic circuit, which in turn depends on the physical profile of its poles. There are two non-active rotor positions: The aligned (when a pair rotor poles is aligned with a pair of stator poles) and the misaligned (when a pair of rotor poles is not aligned with a pair of stator poles). Figure 32 illustrates these situations. The coils inductances of the stator are therefore, bounded by their maximum and minimum values, i.e., rotor and stator pole aligned or rotor and stator pole misaligned, respectively.

Figure 32 – The lining and the misaligned between rotor and poles of the stator

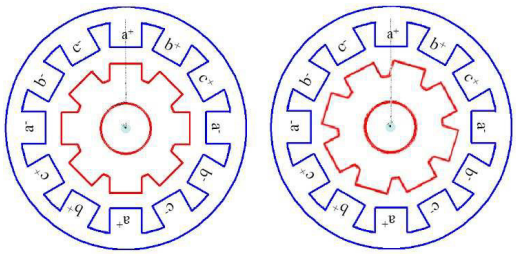

Source: (TEIXEIRA, 2008)

The characteristic of SRM are:

Table 5 – Physical parameters of SRM used

Configuration	12/8
No of phases	3
Nominal Voltage	120V
Nominal Current	9[A]
R	2.4 ohm
Lu	8mH
La	52mH

Source: Author.

Figure 33 – Structure physical of SRM.

Source: <http://www.srdrives.com/land-rover.shtml>

Power up of phases of the SRM is performed through a power converter, where each phase is independently controlled by its own stage of power converter. There are many related studies with power converters for SRM drive systems and many developed topologies for that purpose, each having its advantages and disadvantages (YUAN, 2000; HENRIQUE, 2004). The converter implemented in this work is the Asymmetric Bridge Converter, which is most commonly used for SRM operation. Some authors also use the term classic converter to refer to this topology (VLADIMIRESCU, 1994).

4.3.1.2 Asymmetric Bridge Converter

The implementation of the Asymmetric Bridge Converter to $12/8$ SRM of the laboratory is shown in Figure 34. In this way, the current of the phase i_a, i_b, i_c is maintained around the reference value through the PWM signal whose duty-cycle is determined by the current controller.

Figure 34 – Asymmetric Bridge Converter and SRM

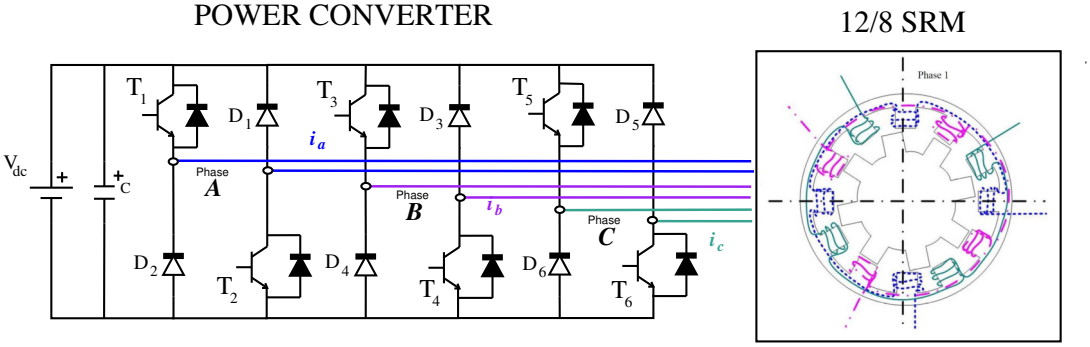

Source: Author

From Figure 34 one may see the asymmetric bridge converter three-phase used in this work. Implementation takes Mosfets of type IRFP460A capable of supporting a drain-source voltage of up to 500 V and 20 A of current, and free wheel diodes ultra fast of type MUR1560 able to withstand up to 600 V and 15 A. However, due to safety reasons, the maximum current is 9 A, which becomes a physical limit to the controller design. Then saturation limits are $\mathrm{U_{max}} = 9[\mathrm{A}]$ and $\mathrm{U_{min}} = 0$.

4.3.1.3 Complete diagram of the prototype

Figure 35 shows the block diagram for the speed control loop of the SRM.

Figure 35 – Overall block diagram of speed loop

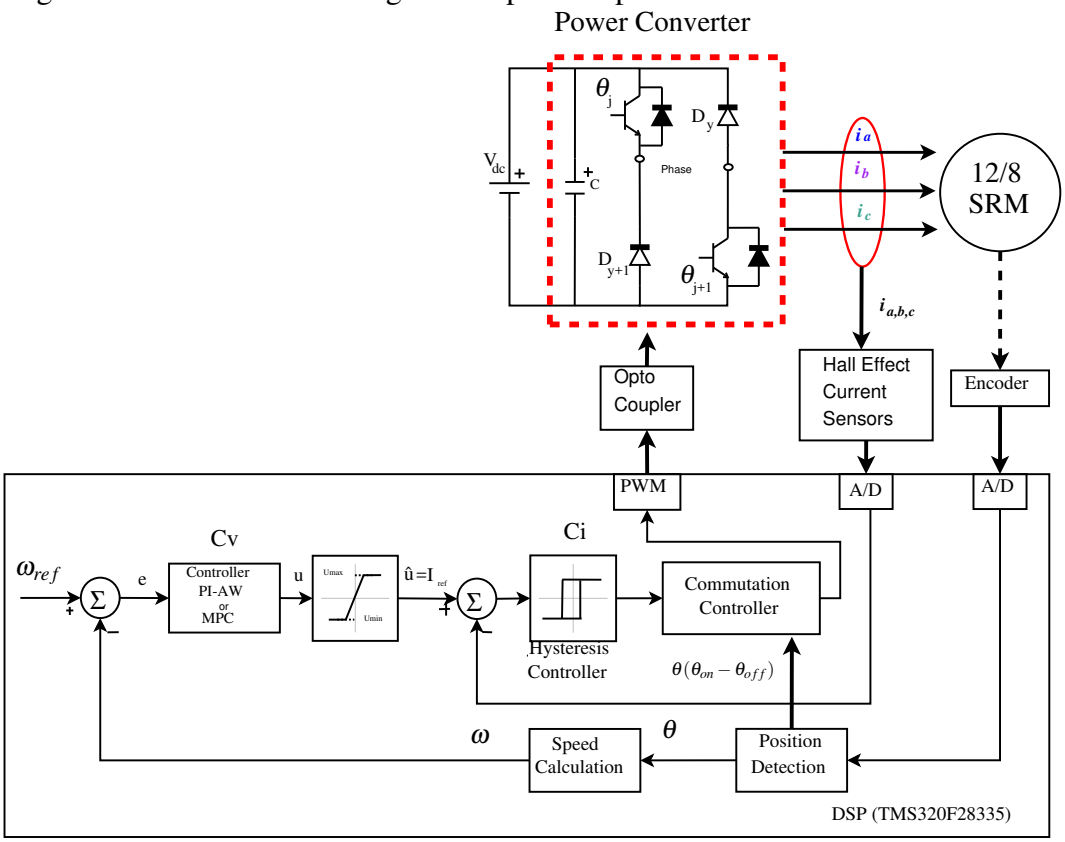

Source: Author

The optocoupler (code 6n136) provides an insulation between the power system and the control system for protection purpose of the latter. In this way, after receiving PWM signals, the optocoupler sends its signals to IR2110, which is responsible for compatibilization with the Mosfet providing a tension in the gate between 12V and 18V.

Take notice that in the physical implementation of the controller, the current loop control signal is characterized by a PWM duty cycle ranging from 0% to 100%, i.e., it is not applied negative control signal. In this way, the ON-OFF control with hysteresis is nothing more than an on and off process of the active phase according to the reference current level and the measured current. A schematic graph of the behavior of the main variables in SRM using this technique is shown in Figure 36 where L_a is the inductance of the phase in the aligned position, L_u is the inductance in the misaligned position, λ_c, is the concatenated flow θ_{on} and θ_{off} are respectively, the ON and OFF phase angles.

Figure 36 – Schematic behavior of the main SRM variables

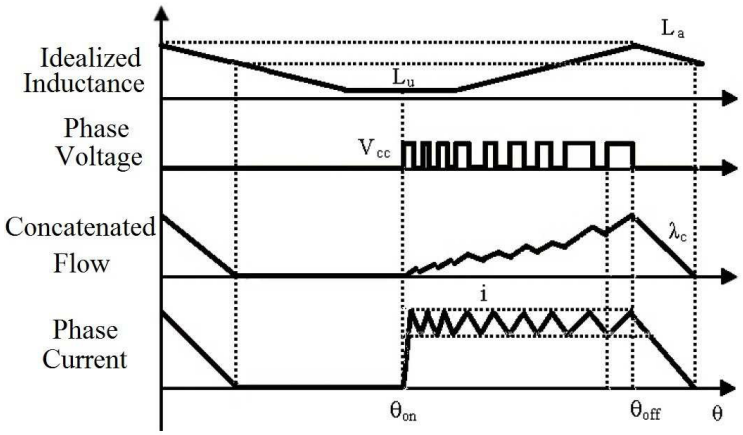

Source: (ALMEIDA, 2007)

Then the control loop that is implemented in the speed control of SRM is:

Figure 37 – Structure of SRM controller

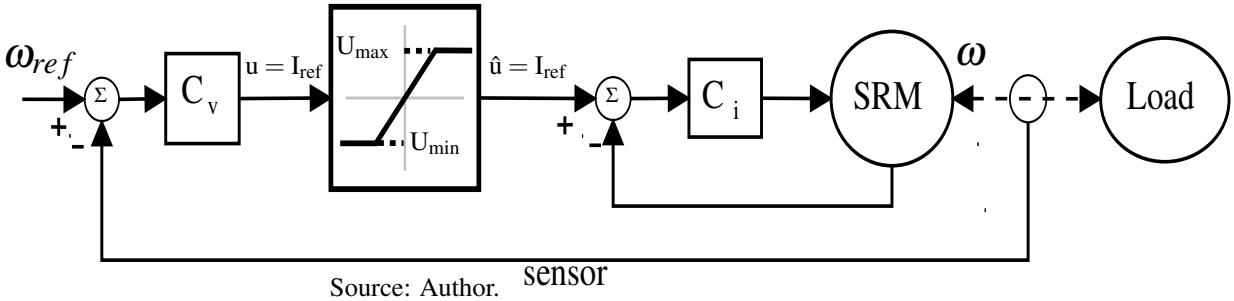

Source: Author.

Figure 38 – Test prototype of SRM speed controller.

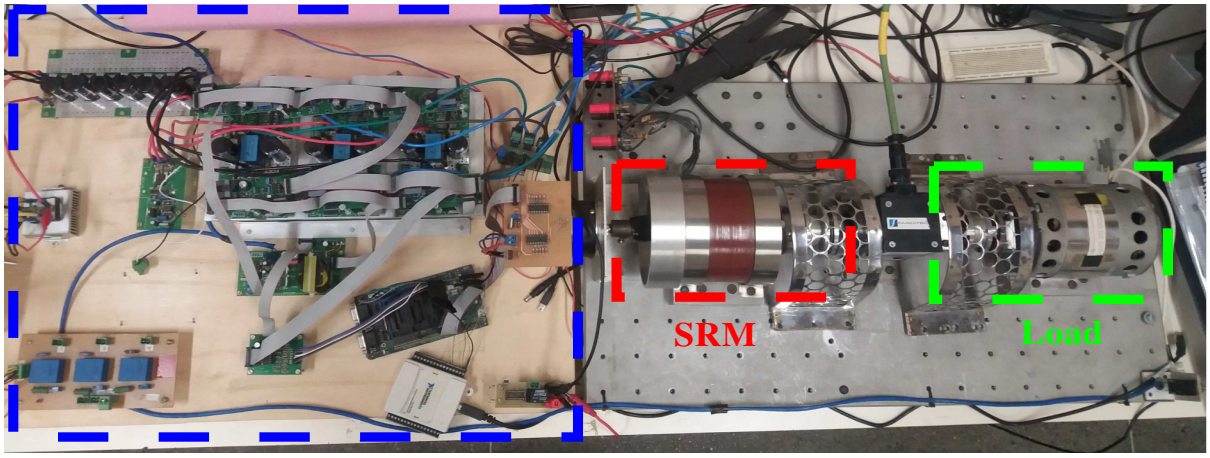

Source: Author.

In Figure 38 one may notice that the SRM is coupled to a generator cascaded with a rheostat, which plays the resistance load role. By varying the resistance one also varies the generator torque which reflects as a load torque disturbance for the reluctance motor. Therefore,

it is considered resistance load in order to get a suitable torque for the speed of the motor. However, the rheostat is manually added to the generator (measured load = 0.8 $[N/m]$).

4.3.2 Modelling of the SRM

The method used is Recursive Least Squares, which consists of an estimation that promotes a minimization of the squares of the differences between an adjusted curve and the values coming from a set of data (AGUIRRE, 2007). The main advantage of this method is to provide a quick identification of easy to interpret and modify.

4.3.2.1 SRM Speed Loop Identification

The speed controller has an inner current control loop and an outer speed control loop. The speed controller generates a signal u, based on the error between the reference speed and actual speed, the which passes by the saturation block, then this signal is $\hat{u} = I_{ref}$, that is reference current. The current in the designated phase is regulated at the reference level by current controller (SILVA *et al.*, 2013; SILVA *et al.*, 2012). The test was performed within a pre-set operating range (between 100 RPM and 1200 RPM) without load coupled at the SRM.

Figure 39 – Overall block diagram of identification SRM of the speed loop

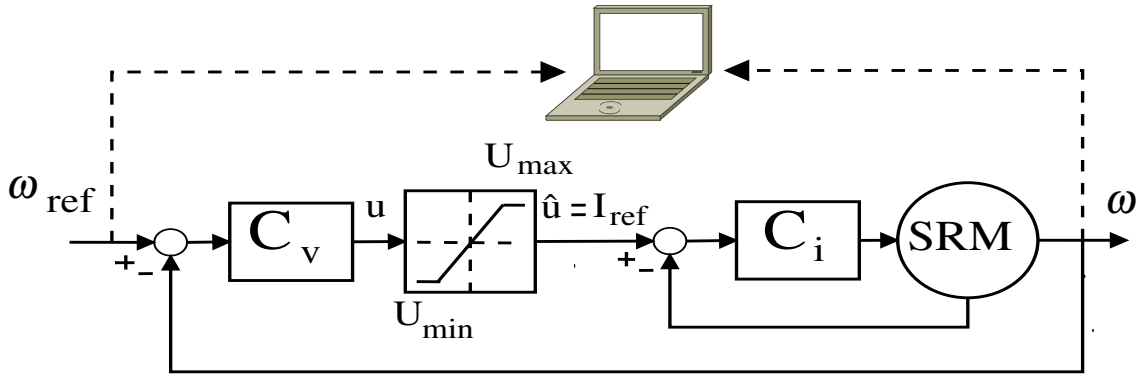

Source: Author.

Note: For input and output data, feedback is not considered and for C_v it remains as a transducer of variable from velocity to current (SILVA, 2017).

As resulted of this identification procedure, the transfer function of SRM loop speed obtained is in time discrete with $C_v = 1$. So the transfer function, that relates speed output and

reference speed input is given by approximation.

$$G(z^{-1}) = \frac{0.032z^{-1}}{1-0.996z^{-1}}. \tag{4.3}$$

According to the equation $G(z^{-1})$ is the transfer function of speed SRM. Where it is observed, that the plant is close to having a behavior of a pure integrator.

4.3.3 Speed controller SRM

In this subsection, it studies the operation of the prototype of test in order to observe how the noise affects under the circumstances already mentioned in a real physical process, between the MPC and PI-AW controllers. The setting of the controllers to compare are as following:

The PI-AW controller design has been considered $K_p = 16.0$, $K_i = 0.8$, $K_{AW} = 0.1$, $T_s = 10e^{-3}[s]$, obtained with the application of the Root Locus method (see subsection 3.1.2.1) along with a fine-tuning based on the simulation of the linear controlled system (without saturation and without Gaussian noise).

The GPC controller it has been set with $T_s = 10e^{-3}[s]$, $\lambda = 0.0$, $N = Nu = 1$, in order to get the same response characteristics in the transient and settling time of the PI-AW. Saturation limits are: $\mathrm{U_{max}} = 9[A]$ and $\mathrm{U_{min}} = 0[A]$ and set-point = 1000 RPM.

4.3.3.1 Results

Initiate the analysis with a simulated response of the SRM speed control, for which the Gaussian noise power measured and calculated using the MatLab software is σ=45 and mean zero, so is introduced in the feedback loop and for the GPC-T controller ($\alpha = 0$), i.e., GPC control.

Figure 40 – Simulated response of SRM speed control

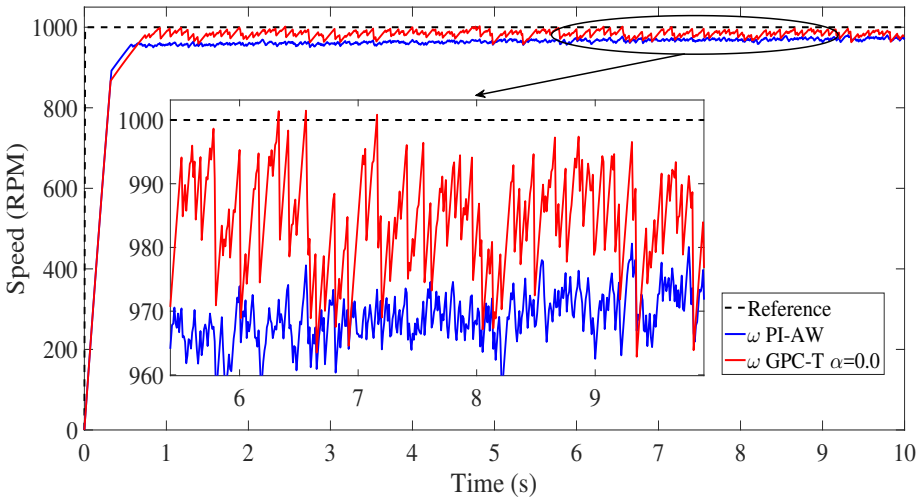

Source: Author.

Figure 41 – Simulated control signal û

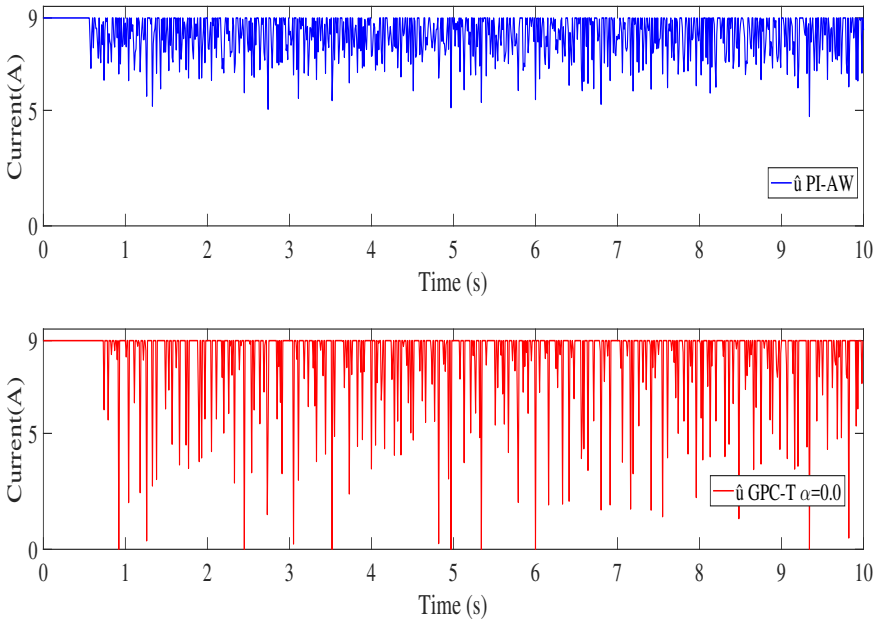

Source: Author.

Figure 40 shows that both controllers present steady-state error, the GPC-T ($\alpha = 0$) presents a smaller error in steady-state, see values in Table 6. It concludes the evidence of NITE phenomenon.

For to corroborate the obtained in the simulations, then it obtains the experimental results.

Figure 42 – Experimental response of SRM speed control

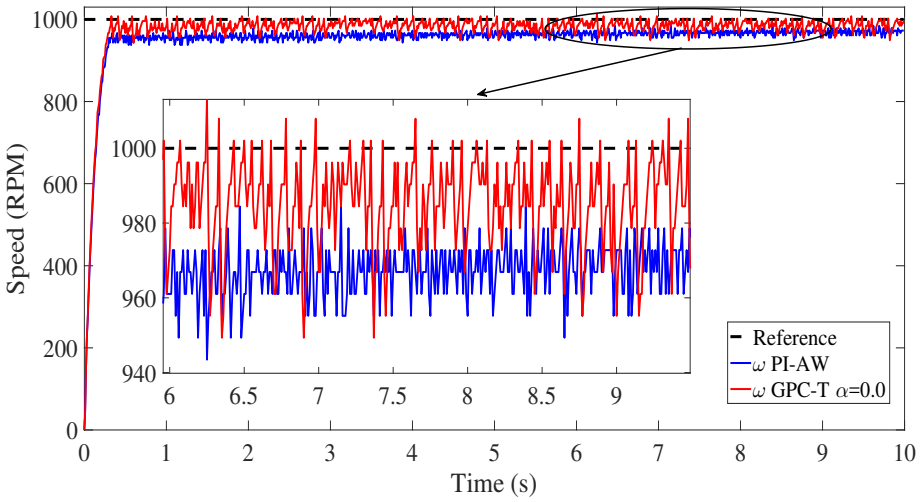

Source: Author.

Figure 43 – Experimental control signal û

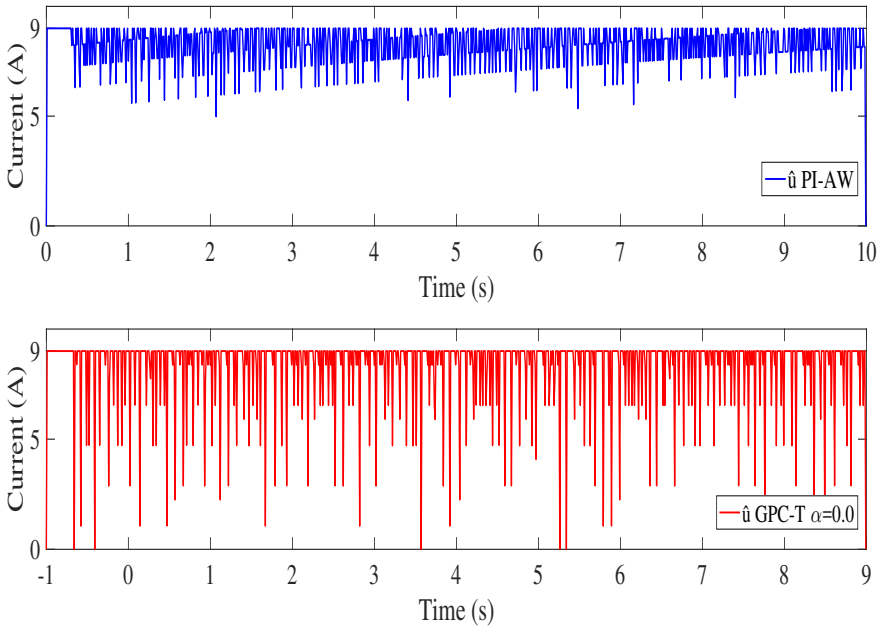

Source: Author.

Figure 42 shows that both controllers present steady-state error, the GPC-T ($\alpha = 0$), see values in Table 6. So It concludes the experimental evidence of NITE phenomenon.

Now proceed to change the value of α for the T-polynomial with $\alpha \to 1$, because this T-polynomial has a compartment of low pass filter.

Figure 44 – Simulated response of SRM speed control ($\alpha \rightarrow 1$)

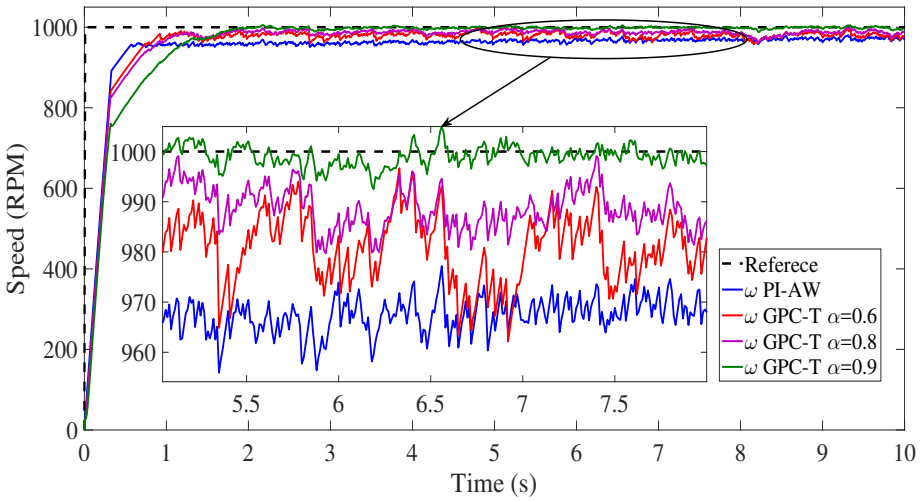

Source: Author.

Figure 45 – Simulated control signal û ($\alpha \rightarrow 1$)

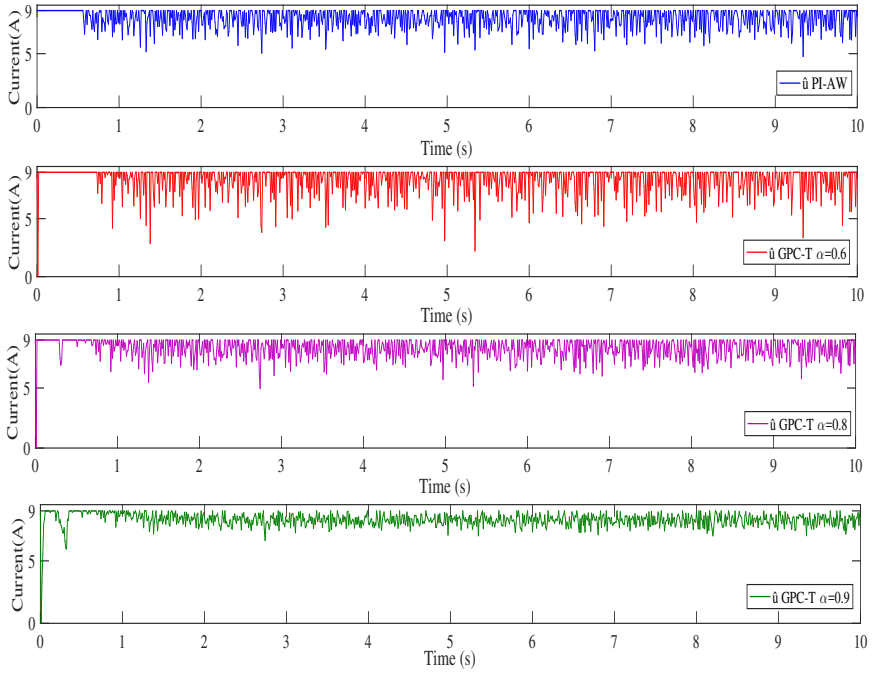

Source: Author.

Figure 44 shows that both controllers present steady-state error and with the GPC-T ($\alpha \neq 0$) presents a decrease of the NITE phenomenon.

For corroborate the obtained in the simulations it proceed to obtain the experimental results.

Figure 46 – Experimental response of SRM speed control ($\alpha \rightarrow 1$)

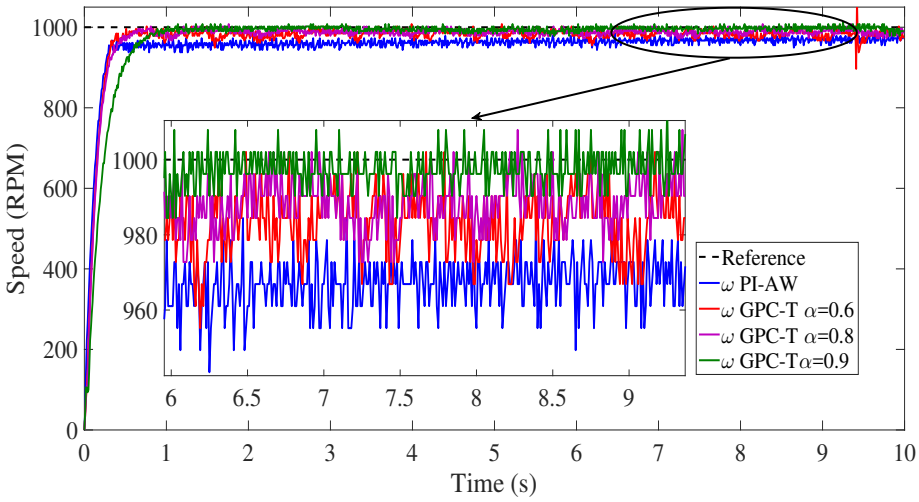

Source: Author.

Figure 47 – Experimental control signal û ($\alpha \rightarrow 1$)

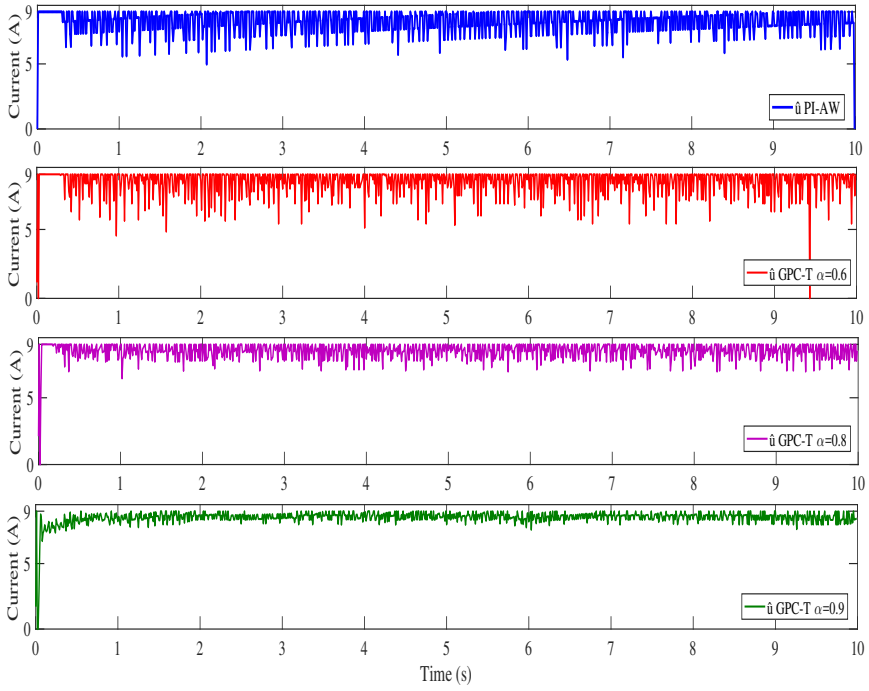

Source: Author

However, Figure 46 shows that both controllers present steady-state error, but as $\alpha \rightarrow 1$, NITE phenomenon is mitigated, as noise peaks become smaller falling in the linear region (see Figure 42). Such a result is compliant with the fact that T-polynomial acts as a low-pass filter, immersed in the calculation of the controller effort (MEGíAS *et al.*, 1997; CAMACHO; BORDONS, 1999).

Table 6 presents comparison results of the performance indices with noise in the feedback loop for PI-AW and GPC-T controllers.

Table 6 – Performance indices of speed control SRM

		Simulated			Experimental		
Controller	α	**IAE**	**TV**(10^3)	$\%e_{ss}$	**IAE**	**TV**(10^3)	$\%e_{ss}$
PI-AW	–	531.3068	1.0008	3.3148	470.1370	9.2870	3.3701
GPC-T	0.0	359.7340	1.3765	1.5995	265.9148	1.3645	3.5536
GPC-T	0.2	373.7386	1.3626	1.7533	332.6282	6.8216	1.5074
GPC-T	0.4	387.9137	1.3168	1.9046	328.5445	9.0560	2.23495
GPC-T	0.6	412.6089	1.2120	1.9400	290.4206	1.0135	2.07702
GPC-T	0.8	364.2784	0.8863	1.2550	255.5334	6.8220	1.6069
GPC-T	0.9	347.6710	0.5032	0.1353	266.6146	3.8733	0.3610

Source: Author.

It is concluded from this analysis, that in the presence of noise (see Table 6), the GPC-T controller ($\alpha = 0.0$) has smaller steady-state error, in comparison with the PI-AW control, by which they have lower performance. Increasing α in GPC-T control until $\alpha = 0.94$, the steady-state error decreases considerably (see Figure 46). Thus, the NITE effect is considerably reduced and its performance is improved relative to the PI-AW.

5 CONCLUSION AND FUTURE WORK

5.1 Conclusion

In the present thesis it studied the implementation of the predictive control algorithm based on a mathematical model, i.e., a GPC-T and compared its performance with a traditional PI-AW controller, applied to different plants. The comparison of these controllers is performed under the presence of Gaussian noise and saturation of the control signal added to the plant. It was observed that this leads to loss of reference tracking, resulting in a steady-state error, therefore as a first conclusion, it is verified the presence of the NITE phenomenon in the MPC Controller.

From the obtained simulations results, it is verified that the predictive control GPC-T $\alpha = 0$, tends to have performance poorer than that of the classic control PI-AW. However, with the incorporation of the T-polynomial, then as second conclusion that is possible to reduce the error in steady state,i.e., decrease the NITE phenomenon. Tuning has been of α is intuitively because the Gaussian noise can vary in power or cannot have access to this measure according to the process.

The GPC predictive controller not only seeks to keep the process at a fixed level, as is the approach of a traditional controller, but also to optimize the resources and maximize the efficiency of the complete system, taking into account imposed constraints,i.e., saturation. In this case, GPC problem is solved through convex optimization.

Experimental results of the speed control of an SRM, as a third conclusion, really demonstrate the presence of the NITE phenomenon and that the implementation time is smaller for the traditional control (PI-AW) compared to the GPC.

The last conclusion is when the GPC-T controller with $\alpha \neq 0$ provides a stable and smooth control signal for the actuator,then to last conclusion is therefore decreases the NITE phenomenon, which allows deducing that there will be an increase in the useful life of the same actuator. It should be considered that the GPC is highly dependent on the plant model, so it should contain as much information as possible on the dynamics of the system.

5.2 Future work

In future work, it is possible to perform an algorithm and choose the most appropriate alpha value in order to make its choice less intuitive. In addition, adaptive controllers may be considered for this study of the NITE phenomenon. Another possible strategy is consider the noise $e(t) \neq 0$ in the predictions of the MPC controller.

BIBLIOGRAPHY

AGUIRRE, L. A. **Introdução à Identificação de Sistemas – Técnicas Lineares e Não-Lineares Aplicadas a Sistemas Reais**. 3. ed. [S.l.]: UFMG, 2007.

ALLGöWER, F.; ZHENG, A. **Nonlinear Model Predictive Control: Progress in System and Control Theories**. 1st. ed. [S.l.]: Birkhäuser Verlag, 2000.

ALMEIDA, R. N. D. C. **Estratégias De Controle De Corrente Para Uma Máquina À Relutância Variável**. Master — Universidade Federal do Ceará, Fortaleza, 2007.

ALMEIDA, R. N. de C.; SILVA, W. A. da; ; TORRICO, B. C.; REIS, L. L. N. dos. Robust control based on generaliza predictive control applied to switched reluctance motor current loop. **Dynamic systems,Measurement, and Control**, ASME, v. 136, n. 3, May 2014.

ANDREWS, L. C. **Special Functions of Mathematical for Engineers**. 2nd. ed. [S.l.]: University Oxford Press, 1998.

ASTRöM, K. J.; HäGGLUND, T. **PID Controllers: Theory, Design, and Tuning**. 2nd. ed. [S.l.]: Instrument Society of America, 1995.

BANERJEE, S.; DAS, S.; KHATU, S.; GUPT, A. Liquid level control system using observer based constrained discrete-time model predictive control. **International Conference on Circuits Power and Computing Technologies (ICCPCT)**, IEEE, October 2017.

BORDIGNON, V. **Controle Preditivo Multivariável Aplicado a uma Planta De Nível**. Graduation — Universidade Federal Do Rio Grande Do Sul, 2016.

CAMACHO, E. F.; BORDONS, C. **Model Predictive Control**. 2nd. ed. [S.l.]: Springer, 1999.

CLARKE, D. W.; MOHTADI, C.; TUFFS, P. S. Generalized predictive control-part i. **Automatic**, n. 23, p. 137–148, 1987.

COHEN, G. H.; COON, G. A. Theoretical consideration of retarded control. ASME, v. 75, n. 1, p. 827–834, August 1983.

DIAS, S. V. **Controlador Preditivo Generalizado Com Anti-Windup Aplicado A Um Sistema De Geração Eólico Baseado Em DFIG**. Ph.D — Universidade Federal do Ceará, Fortaleza, 2016.

DIAS, S. V.; SILVA, W. A. da; ; TORRICO, B. C.; REIS, L. L. N. dos. Robust generalized predictive control applied to the mitigation of electromagnetic torque oscillations in a wind energy conversion system based on dfig. **Biennial Congress of Argentina (ARGENCON)**, IEEE, Oct 2016.

DORF, R. C.; BISHOP, R. H. **Modern Control Systems**. 12th. ed. [S.l.]: Prentice Hall, 2011.

EUN, Y.; S., H. E. Noise induced loss of tracking in systems with saturating actuators and antiwindup. **Journal of Dynamic Systems, Measurement, and Control**, ASME, v. 136, Sept 2015.

FERTIK, H. A.; ROSS, C. W. Direct digital control algorithm with anti-windup feature. **ISA Transactions**, v. 6, p. 317–328, 1967.

GUERRERO, V.; MARTíNEZ, L.; YUSTE, R. L. **Industrial Communications**. 1st. ed. [S.l.]: Alfaomega Marcombo, 2009.

HANSLER, E.; SCHMIDT, G. **Acoustic Echo and Noise Control**. 1st. ed. [S.l.]: A JOHN WILEY & SONS, 2004.

HENRIQUE, L. O. de A. P. **Implementacao de Estrategia de Minimizacao de Oscilacao de Torque Usando Controle Neuro-Fuzzy e Remocao de Sensor de Posicao para um Acionamento de Relutancia Variavel**. Ph.D. — Universidade Federal do Rio do Janeiro, Janeiro, 2004.

HU, T.; LIN, Z. **Control Systems with Actuator Saturation, Analysis and Design**. 1st. ed. [S.l.]: Birkhäuser Basel, 2001.

HU, T.; LIN, Z. **Control Systems with Actuator Saturation, Analysis and Design**. 1st. ed. [S.l.]: Springer Science Business Media, 2001.

HUANG, Y.; LI, Y.; LIU, X.; SHEN, J. Industrial application of constrained mpc with zone control to a coupled flue gas desulfurization system. **Chinese Automation Congress (CAC)**, IEEE, October 2017.

INFINEON. **Applications of SRM**. 2017. Disponível em: <https://www.infineon.com/cms/en/applications/>. Acesso em: 28 jun. 2017.

KIM, D.; K., P.; EUN, Y.; SON, S. H.; CHENYANG, L. When thermal control meets sensor noise:analysis of noise-induced temperature error. **IEEE Transactions on Industry Applications**, IEEE, 2015.

KOTHARE, M. **Control of Systems Subject to Constraints**. Master — California Institute of Technology, 1997.

KRISHNAN, R. **Switched Reluctance Motor Drives: Modeling, Simulation, Analysis, Design and Application**. 1st. ed. [S.l.]: Industrial Electronics Series, 2001.

LAMBERT, M. R. **Adaptive Control of Flexible Systems**. Ph.D — University of Oxford, 1987.

LEE, J.; EUN, Y. Analysis of noise-induced tracking loss in pi controlled systems with anti-windup. **American Control Conference**, ACC, p. 5461–5466, July 2016.

LI, Y. **Predictive Control for Dynamic Systems to Track Unknown Input In the Presence of Time Delay**. Master — University of Central Florida, 2005.

LOPEZ, A. M.; MILLER, J. A.; SMITH, C. L.; MURRIL, P. Tuning controllers with error-integral criteria. **Instrumentation Technology**, p. 57–62, 1976.

MCINTOSH S. L. SHAH, D. G. F. A. R. Analysis and tuning of adaptive generalized predictive control. **The Canadian Journal of Chemical Engineering**, v. 69, n. 1, p. 97–110, 1991.

MEGíAS, D.; SERRANO, J.; PRATA, C. de. Undertainty treatment in gpc: Design of t polynomial. **European Control Conference**, ECC, Sept 1997.

MOHAMMED, J. A. S. Measurement of vibration and noise level at power plant and refinery companies that represents a condition monitory for the health of machines. **International Conference on Environment Impacts of the Oil and Gas Industrie (EIOG)**, IEEE, April 2017.

NUNES, G. C. **Design and Analysis of Multivariable Predictive Control Applied to an Oil-Water-Gas Separator**. Graduation — University of Florida, 2001.

OGATA, K. **Modern Control Engineering**. 3rd. ed. [S.l.]: Prentice Hall, 1997.

OGAWA, H.; SASAKI, K.; TSUMOTO, K. M.; ISHIDA, Y. A simple antiwindup control based on a pi control with an initial value of the integral state variable. Computer and Automation Engineering (ICCAE), Feb. 2010.

RAHMAN, K.; FAHIMI, B.; VELAYUTHAM, A. Advantages of switched reluctance motor applications to ev and hev: Design and control issues. **IEEE Transactions on Industry Applications**, IEEE, v. 36, n. 1, Jan 2000.

RAMAKRISHNAN, K. Delay-dependent stability of generator-excitation control system using root-locus approach. **Trends in Industrial Measurement and Automation (TIMA)**, IEEE, Jane 2017.

ROJAS, J. **Extension and Applications of the Virtual Reference Feedback Tuning**. Ph.D — Universidad Autonoma de Barcelona, 2011.

SAKAI, K.; ISHIDA, Y. A design of an improved anti-windup control using a pi controller based on a pole placement method. **International Journal of Simulation Systems, Science & Technology**, ijssst, v. 17, n. 34, 2016.

SHIN, H. B.; PARK, J. G. Anti-windup pid controller with integral state predictor for variable-speed motor drives. **IEEE Transactions on Industry Applications**, IEEE, v. 59, n. 3, March 2012.

SHORT, M.; ABUGCHEMN, F. A micro controller-based adaptive model predictive control platform for process control applications. **electronics**, v. 6, n. 88, 2017.

SILVA, W. A.; CARVALHO, R. N. de; TORRICO, B. C.; REIS, L. N. dos. Spees and current control in switched reluctance motor based on pid and generalized predictive control. **Congresso Regional de Iniciação Científica e Tecnológica em Engenharia**, iREP, n. 1892, Sept 2012.

SILVA, W. A. D. **Controle Preditivo Aplicado Às Malhas De Corrente E Velocidade De Um Sistema De Acionamento Com Motor De Relutância Variável**. Master — Universidade Federal do Ceará, Fortaleza, 2013.

SILVA, W. A. da. **Controle de Máquina de Relutância Variável em Situação de Falta de Fase**. Ph.D. — Universidade Federal do Ceará, Fortaleza, 2017.

SILVA, W. A. de; REIS, L. N. dos; TORRRICO, B. C.; CARVALHO, R. N. de. Speed control in switched reluctance motor based on generalized predictive control. **Power Electronics Conference**, COBEP, Sept 2013.

SIMKOFF, J. M.; WANG, S.; BALDEA, M.; CHIANG, L. H. Plant-model mismatch evaluation for unconstrained mpc with state estimation. **Decision and Control (CDC)**, IEEE, December 2017.

STEIN, G. **Bode lecture: Respect the unstable**. [S.l.]: In Proceedings of the 28th IEEE Conference on Decision and Control, Tampa, Florida, 1989.

TEIXEIRA, V. S. D. C. **Análise Da Operação De Sistemas De Ventilação Industrial Visando À Eficiência Energética**. Master — Universidade Estadual do Ceará, Fortaleza, 2008.

TURSINI, M.; VILLANI, M.; FABRI, G.; LEONARDO, L. D. A switched-reluctance motor for aerospace application: Design, analysis and results. **Electric Power Systems Research**, n. 142, p. 74–83, Sept 2016.

VISIOLI, A. **Practical PID Control**. 1st. ed. [S.l.]: Springer-Verlag London Limited, 2006.

VLADIMIRESCU, A. **The SPICE Book**. [S.l.]: John Wiley & Sons, 1994.

YUAN, G. **Speed Control of Switched Reluctance Motors**. Master — Hong Kong University of Science and Technology, 2000.

ZIEGLER, J. G.; NICHOLS, N. B. Optimum settings for automatic controllers. **The American Society of Mechanical Engineers**, ASME, v. 64, n. 1, 1942.